Reconstructing Palaeoarchaean microbial biomes flourishing in the presence of emergent landmasses using trace and rare earth element systematics

Reconstructing Palaeoarchaean microbial biomes flourishing in the presence of emergent landmasses using trace and rare earth element systematics

Keyron Hickman-Lewis[a,b,*], Blandine Gourcerol[c], Frances Westall[b], Daniela Manzini[d], Barbara Cavalazzi[a,e]

[a] *Dipartimento di Scienze Biologiche, Geologiche e Ambientali (BiGeA), Università di Bologna, via Zamboni 67, I-40126 Bologna, Italy*
[b] *CNRS Centre de Biophysique Moléculaire, Rue Charles Sadron, F-45071 Orléans, France*
[c] *BRGM, F-45060 Orléans, France*
[d] *Centro Interdipartimentale Grandi Strumenti (CIGS), Università di Modena e Reggio Emilia, 213A via Giuseppe Campi, Modena, Italy*
[e] *Department of Geology, University of Johannesburg, PO Box 524, Auckland Park 2006, Johannesburg, South Africa*

A B S T R A C T

Palaeoarchaean cherts preserve the most ancient direct traces of life, but this palaeobiological testament is rarely assimilated into ecosystem or biome models. Trace and rare earth element plus yttrium (REE + Y) compositions reliably decode the palaeodepositional settings of these cherts, and thus constrain the environments within which early microbial life flourished. Herein, we present systematic comparisons between bulk inductively coupled plasma mass spectrometry (ICP-MS) of four fossiliferous cherts from the Barberton greenstone belt, South Africa (the 3.472 Ga Middle Marker horizon, 3.45 Ga Hooggenoeg H5c chert, 3.334 Ga Footbridge Chert, and ~3.33 Ga Josefsdal Chert), and *in situ* laser ablation (LA) ICP-MS transects through microbial laminations therein. Normalised bulk ICP-MS analyses generally exhibit fractionated REE + Y patterns typical of anoxic hydrogenous sedimentation, supporting previous assertions that the Palaeoarchaean habitable realm was a hydrothermally influenced ocean. Suppressed La, Eu and Y anomalies, together with supra-chondritic Y/Ho ratios, however, indicate restriction from the open ocean and influences from non-marine waters. *In situ* LA ICP-MS transects through fossiliferous layers yield flat, light REE-enriched REE + Y patterns and chondritic Y/Ho ratios indicating major contributions from terrigenous, riverine fluids, i.e. continental weathering. Resurgences of marine chemistry (increased Y/Ho ratios, La and Y anomalies) occur within microbial laminations themselves. Combined, these results evidence the presence of emergent, volcanic landmasses in the Palaeoarchaean, and highlight the importance of epicontinental basins atop these landmasses as loci for microbial biomes up to 250 Ma before large-scale terrestrial ecosystems. Increased riverine weathering of mafic-felsic continental ma-terial, together with periodic seawater recharge into these basins, generated disequilibrium redox conditions under which microbial life flourished. Emergent landmasses may thus have catalysed the flourishing of widespread productive photosynthetic biomes. Charting the relative dominance of biomes through time could illu-minate microbial evolutionary trajectories through the lens of environmental reconstruction. Furthermore, we advocate the use of correlated bulk and *in situ* geochemical approaches in reconstructing ancient environments, since signals relating to small-scale palaeoenvironmental fluctuation can evidently be masked by bulk rock chemistry.

1. Introduction

Quantitative and semi-quantitative geochemical tools capable of constraining local- and regional-scale palaeoenvironments on the early Earth are of paramount importance in elucidating the co-evolution of the geosphere and biosphere. The palaeodepositional environments of silicified Archaean metasediments (cherts) are reliably archived within their rare earth element plus yttrium (REE + Y) compositions (Bau and Dulski, 1996; Kamber and Webb, 2001; Kato and Nakamura, 2003; Bolhar et al., 2004; Kamber et al., 2004; Bolhar and Van Kranendonk, 2007; Sugahara et al., 2010; Allwood et al., 2010; Gourcerol et al., 2015, 2016). Biogeochemical signatures within cherts are well-preserved by virtue of the early and rapid 'time capsule' preservation afforded by silicification, where post-diagenetic alteration is very minor

compared to carbonates, evaporites and volcaniclastics (Westall et al., 2011, 2015; Hickman-Lewis et al., 2017). Indeed, silicification occurs sufficiently ea rly an d ra pidly th at mi crofossils, mi crobial ma ts and other organo-sedimentary fabrics can be preserved in volume during life processes (e.g. Knoll and Barghoorn, 1977; Walsh, 1992; Tice and Lowe, 2006a; Westall et al., 2011, 2015; Hickman-Lewis et al., 2017, 2018a; Greco et al., 2018). This suggests that the timescale of silicification may be less than weeks to months, beginning within hours; indeed, experimental silicification of prokaryotes validates that the process begins w ithin24 h (Bartley, 1996; Orange et al., 2009). Precambrian sediments can thus archive their depositional regimes over very short timescales, such that REE + Y compositions fluctuate pre-dictably betwe en microband/layer deposition (Bau and Dulski, 1996; Tice and Low e, 2006b; Allw ood et al., 2010; Sugahara et al., 2010; Gourcerol et al., 2015, 2016; Ledevin et al., 2019), and have the po-tential to preserve geochemistry on timescales relevant to microbial grow th. The MuQ-normalised REE + Y composition of aqueous re-servoirs has been relatively constant since the Archaean. For marine reservoirs, this typically includes positive La, Gd and Y anomalies and an enrichment of heavy REE (HREE) over light REE (LREE) (Bolhar et al., 2004, 2015; Shields and Webb, 2004). Archaean marine pre-cipitates do not exhibit negative Ce anomalies due to the prevailing anoxic conditions in the early oceans being reducing with respect to the Ce^{4+}/Ce^{3+} couple (Kamber et al., 2004; Bolhar et al., 2015), but show pronounced Eu anomalies attributed to hydrothermal signals advected throughout the w ater column (Danielson et al., 1992; Hofmann and Harris, 2008). Characteristic REE + Y patterns can therefore be in-ferred to represent similar aqueous geochemical processes throughout geological time (Shields and Webb, 2004).

Delineating the aqueous chemistries defining multiple fossiliferous horizons throughout the Archaean would ameliorate our understanding of the evolution of biogeochemistry in deep time. The task facing this work is thus defining and applying an approach for the reconstruction of microbial biomes on the Palaeoarchaean Earth using REE + Y chemistry to characterise the palaeoenvironments inhabited by early life at multiple resolutions (Fig. 1A).

1.1. Building a biome model of the Palaeoarchaean: Review and perspectives

The Barberton greenstone belt, southern Africa, and the East Pilbara terrane, Western Australia, are the oldest w ell-preserved sedimentary successions w ithin w hich are recognised convincing traces of life as-sociated w ithdiscernible palaeoenvironments (e.g. Wacey, 2009; Brasier et al., 2011; Hickman-Lewis et al., 2018b). Many well-preserved biosignatures from these successions manifest themselves as organo-sedimentary structures, including stromatolites, biolaminites and mi-crobial mats. Although it is challenging to infer a microbial ecosystem based solely on palaeontological evidence, similarities betw een fossil and modern microbial mat morphologies and their occurrence in rocks reflecting s hallow -w ated eposition s uggest t hat a noxygenic photo-synthetic microbial communities w ereal ready flourishing by 3.4–3.5 Ga (Walsh and Lowe, 1999; Nisbet and Fowler, 1999; Tice and Lowe, 2006a; Allwood et al., 2009; Westall et al., 2011, 2015; Noffke et al., 2013; Schopf et al., 2017; Hickman-Lewis et al., 2016, 2018a,b, 2019; Greco et al., 2018).

Numerous environmental niches w ere colonised by around 3.5 Ga (Brasier et al., 2011; Knoll et al., 2016) and presumably formed a globally co-operative biosphere (Nisbet, 1995). Anoxygenic submarine platforms w ere seemingly w idely colonised (see references above), how ever, there is similarly evidence for life in periodically or continually exposed terrestrial environments (Westall et al., 2011; Djokic et al., 2017; Homann et al., 2018) and possibly within the water column (Walsh, 1992; Oehler et al., 2017; Sugitani, 2018). Ichnofossils from the Archaean remain contentious despite resembling modern bacterial al-teration textures, and there is therefore less constraint on the subsurface biosphere (Furnes et al., 2004, 2007). Our foci herein are the widespread, presumably phototrophic microbial mats (preserved as biolaminites; Fig. 2, S1–S2) which, having large areal distribution and occurring at the geosphere-hydrosphere-atmosphere interface, were likely the major drivers of biogeochemistry on the early Earth (Nisbet and Fowler, 1999; Lenton and Daines, 2016).

To reconstruct this anoxygenic photosynthetic Archaean biome, microbially influenced horizons from four cherts spanning approximately 150 Ma of the Palaeoarchaean of the Barberton greenstone belt w ere analysed: the 3.472 Ga Middle Marker horizon, the ~3.45 Ga Hooggenoeg chert H5c, the 3.334 Ga Footbridge Chert and the ~3.33 Ga Josefsdal Chert (Figs. 2 and 3). These cherts are sedimentary horizons deposited by the precipitation of silica directly from silica-supersaturated seawater (Tice and Lowe, 2006a,b; Ledevin et al., 2014), from w ater-rock dissolution reactions, and/or from hydrothermal venting and circulation (Danielson et al., 1992; Hofmann and Harris, 2008; Ledevin et al., 2014; Westall et al., 2015). Barberton cherts occur immediately above zones of progressive silicification of the underlying volcanic-volcaniclastic sequences (Hofmann and Bolhar, 2007; Hofmann and Harris, 2008; Hofmann, 2011). These silicification zones are interpreted as resulting from diffuse, low -temperature hydrothermal circulation of seawater in an oceanic plateau-like setting (Kato and Nakamura, 2003; Bolhar et al., 2004; Hofmann and Harris, 2008). Hydrothermal convection cells beneath chert horizons were initiated by high regional heat flow and the cooling and dissolution of volcanic rock, and imply that the overlying seaw ater-sediment interface was warm-hot (Hofmann and Bolhar, 2007). Previous trace and rare earth element studies into the settings represented by such fossiliferous cherts in the Barberton region have, how ever, painted a relatively homogeneous, marine-dominated, picture throughout the Palaeoarchaean and Mesoarchaean. The absence of a negative Ce anomaly denotes anoxic conditions (*cf*. Bau and Dulski, 1996; Kamber and Webb, 2001), w hereas some limited LREE enrichment, together w ith unsilicified phases, illustrate variable detrital sources of mafic, dacitic and felsic compositions contributing to the clastic component in cherts (Lowe, 1999; Kato and Nakamura, 2003; Hofmann et al., 2013; Ledevin et al., 2014). The relative contributions of these sources have not yet been determined, but their significance relative to hydrogenous precipitation is assumed to be minor such that deposition is envisaged in environments dominated by the influence of the open ocean (e.g., Hofmann and Wilson, 2007; Hofmann and Harris, 2008; Westall et al., 2015; Hickman-Lewis et al., 2018a). Similar w ork on contemporaneous fossiliferous horizons from the East Pilbara terrane, including the 3.481 Ga Dresser Formation and the 3.43 Ga Strelley Pool Formation, shows a less complex scenario, w ith dominantly w ell-fractionated REE + Y patterns indicating that these horizons formed under typical open ocean Archaean hydrogenous sedimentation (Van Kranendonk et al., 2003; Allwood et al., 2010), although Kato and Nakmura (2003) found evidence for locally exposed granitoids in the Marble Bar greenstone belt. These bulk geochemistries are assumed to be relevant to the environment of early life, how ever, the petrological context of the geochemistry w ith respect to fossiliferous horizons has received little investigation.

Widespread evidence for significant continental (terrigenous) weathering inputs is hardly seen in fossiliferous cherts and carbonates until the Mesoarchaean and Neoarchaean, the sole w ell-explored example being that of the locally exposed granitoids of Marble Bar reported by Kato and Nakamura (2003). Grassineau et al. (2002) found that limestones in the 2.7 Ga Belingwe greenstone belt (Zimbabwe) had LREE-rich REE + Y patterns controlled by locally sourced coastal material. Kamber et al. (2004) measured stromatolitic carbonates from the 2.7 Ga Mushandike Limestone (Zimbabw e) with a negative REE + Y slope in spite of positive La and Gd anomalies and a superchondritic Y/Ho ratio, and similarly suggested deposition in a restricted epicontinental sea with strong influence from local LREE-enriched continents. Contemporaneous stromatolitic carbonates from the Fortescue Group

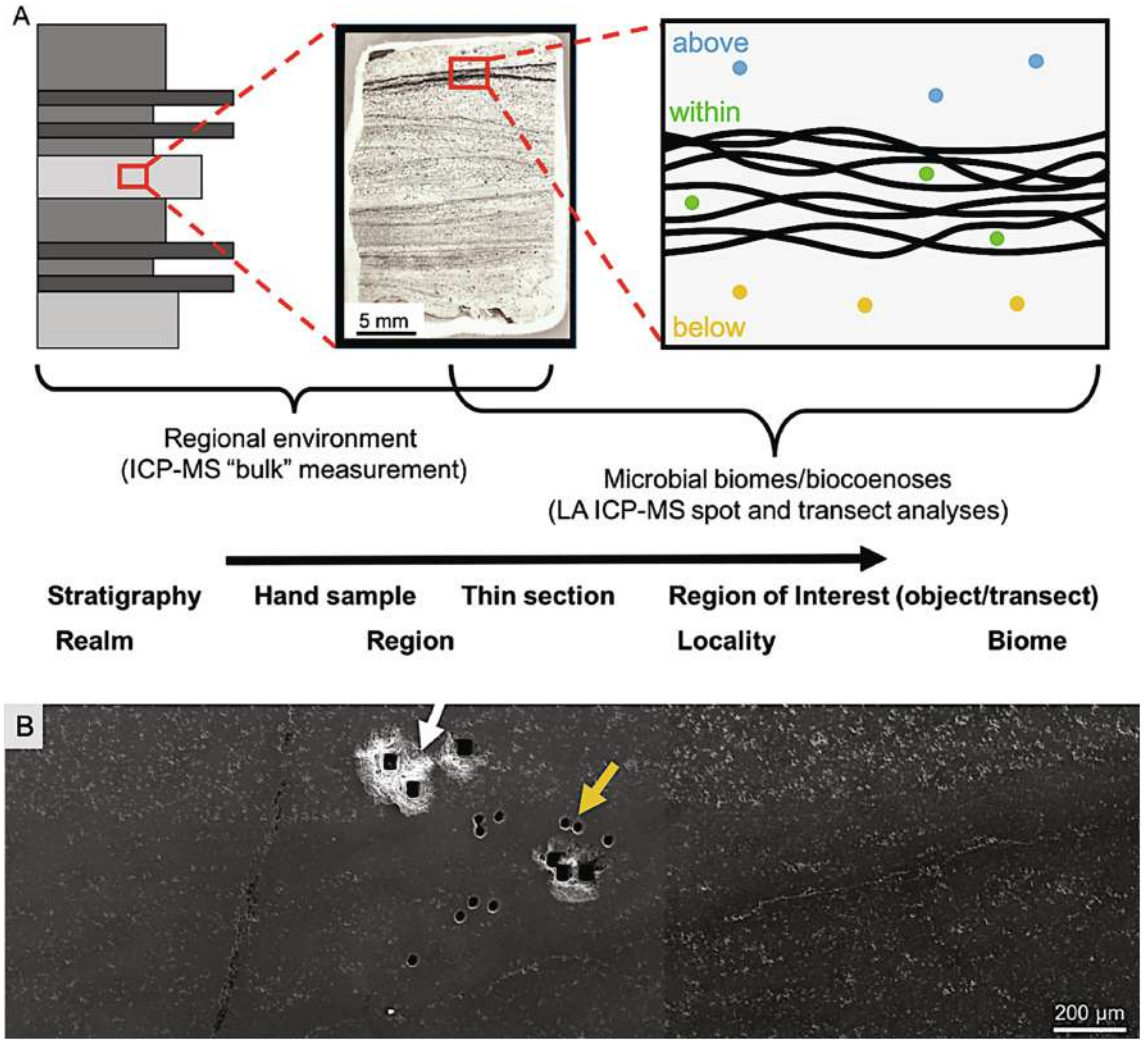

Fig. 1. A) Analytical approach linking bulk ICP-MS and *in situ* LA ICP-MS measurements to their palaeoenvironmental context. Bulk ICP-MS analyses of hand samples, with respect to stratigraphic and outcrop context, decode regional-scale environments. These findings can be linked to thin section petrography. *In situ* LA ICP-MS spots (coloured points) and transect (a sequence of points) analyses within thin sections link the local environment and biome-scale geochemistry that accompanies the flourishing of microbial ecosystems. Transects were taken across mat-bearing horizons as shown in the schematic, incorporating the cherts above, within and below the mats as shown by the yellow, green and blue points. These analyses are reciprocatively linked to thin section petrography and can thus be placed within local and regional palaeoenvironmental contexts. **B**) SEM micrograph showing transect of LA ICP-MS point analyses through a microbial mat. Spot analyses are 65 µm (white arrow) or 40 µm (yellow arrow) depending upon the size of the analysed region of interest. (For interpretation of the references to colour in this figure legend, the reader is referred to the web version of this article.)

(Pilbara) exhibit flat REE + Y patterns, lack La and Gd anomalies, and have supra-chondritic Y/Ho ratios, leading Bolhar and Van Kranendonk (2007) to interpret their palaeodepositional setting as lagoonal-lacustrine and dominated by freshwater influx. Sugahara et al. (2010) and Bolhar et al. (2015) studied 3.0–2.9 Ga horizons from the Pongola Supergroup (southern Africa) and Mount Goldsworthy greenstone belt (Western Australia), finding variable influence from continental sources. Sugahara et al. (2010) noted MREE enrichment, chondritic to supra-chondritic Y/Ho values and La anomalies in black cherts associated with evaporites that they interpreted to have formed in water masses influenced by continental run-off into the open ocean, with negligible hydrothermal influence. Chemical and clastic sedimentary rocks of the Pongola Supergroup also exhibit LREE and MREE enrichment and show suppressed La, Gd, Y and Eu anomalies that suggest deposition in a restricted basin with fluctuating, but generally restricted, exchange with the open ocean (Bolhar et al., 2015). Other stromatolitic carbonates and iron formations of the Mesoarchaean-Neoarchaean show REE + Y patterns typical of marine deposition (e.g., Bau and Dulski, 1996; Kamber and Webb, 2001). Stüeken et al. (2015, 2017) studied the metabolic networks of Neoarchaean lacustrine systems, showing that these systems developed atop Late Archaean continents and, most recently, Homann et al. (2015, 2018) described the well-preserved shoreface and terrestrial ecosystems in the 3.22 Ga Moodies Group. The fact that both continentally influenced and marine-dominated aqueous geochemistries and microbial consortia are found in Mid-Late Archaean sediments indicates that microbial biomes had, by this time, expanded into numerous tectonic settings with areally extensive distinctions between oceanic and continentally dominated ecosystems, likely as a result of the emerging continental crust around this time (Cawood et al., 2018). Whether this was already the case in the Early Archaean remains an unanswered question.

Each chert analysed in this study represents a habitable environment with unequivocal microbial communities, which can be reconstructed with increasing specificity using bulk and laser ablation (LA) inductively coupled plasma mass spectrometry (ICP-MS) (Fig. 1). Multiple scales of analysis are critical in determining the precise nature of the co-evolution of life and environments since the use of bulk measurements alone can mask significant enrichments or depletions in

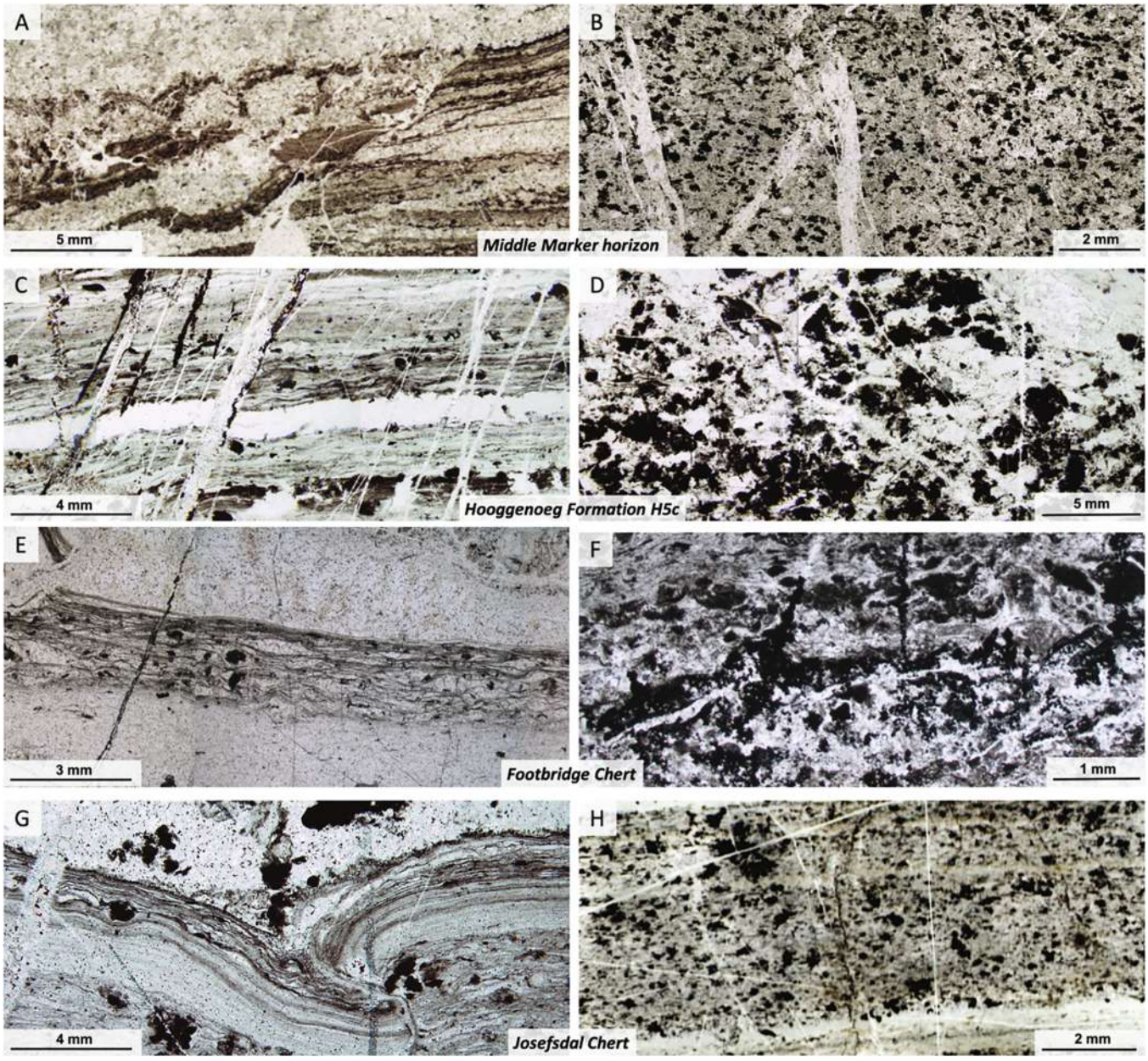

Fig. 2. Petrographic detail of some of the studied samples, demonstrating the similarity of their organo-sedimentary textures. Further photomicrographs are presented in the Supplementary Material. **A**) Silicified sediments from the Middle Marker horizon characterised by a thick set of micro-tufted microbial mats (sample 07SA23). The mats are preserved poorly, and distended, at the left-hand side of the image, but show excellent preservation of micro-tufts at the right-hand side. **B**) Massive, structureless black chert from the Middle Marker horizon, comprising matrix-supported carbonaceous particles (sample 07SA22). **C**) Laminated black and white chert from Hooggenoeg Chert H5c, showing well-preserved mat laminations intercalated with near-pure silica layers (sample 03SA15). **D**) Massive, clotted carbonaceous chert from Hooggenoeg Chert H5c (sample 03SA04). **E**) Exquisitely preserved microbial mat from the Footbridge Chert, overlain by granular carbonaceous sediment layers (03SA09). **F**) Weakly laminated, massive chert from the Footbridge Chert (sample 03SA09′). **G**) Deformed, finely laminated microbial biofilms from the Josefsdal Chert (sample 12SA18). **H**) Weakly laminated clotted carbonaceous chert from the Josefsdal Chert (sample 99SA07).

trace element concentrations at finer scales (Robbins et al., 2019). Herein, the following scales are considered:

- 'regional', combining sedimentological observations with bulk ICP-MS data (spanning a scale of macroscopic observation from stratigraphy to hand sample);
- 'local', combining bulk ICP-MS data and *in situ* LA ICP-MS data from the stratigraphy immediately surrounding microbial horizons (from hand sample to thin section); and
- 'biome', by conducting *in situ* LA ICP-MS transect analyses through microbial layers (spanning a scale from thin section to only several millimetres within, directly related to microbial activity). This highest resolution of analysis resolves aqueous chemistry on the short timescales during w hich microbial ecosystems flourished (Fig. 1).

1.2. REE + Y geochemistry as an indicator of palaeoenvironment: Interpretation and consideration

Trace and REE + Y compositions of cherts are determined by their concentration both w ithin quartz (e.g., Kato and Nakamura, 2003; Kamber et al., 2004) and carrier phases, such as Fe-Mn oxyhydroxide particles, that have undergone variable silicification (e.g., Hofmann et al., 2013; Ledevin et al., 2014; Gourcerol et al., 2015; Bolhar et al.,

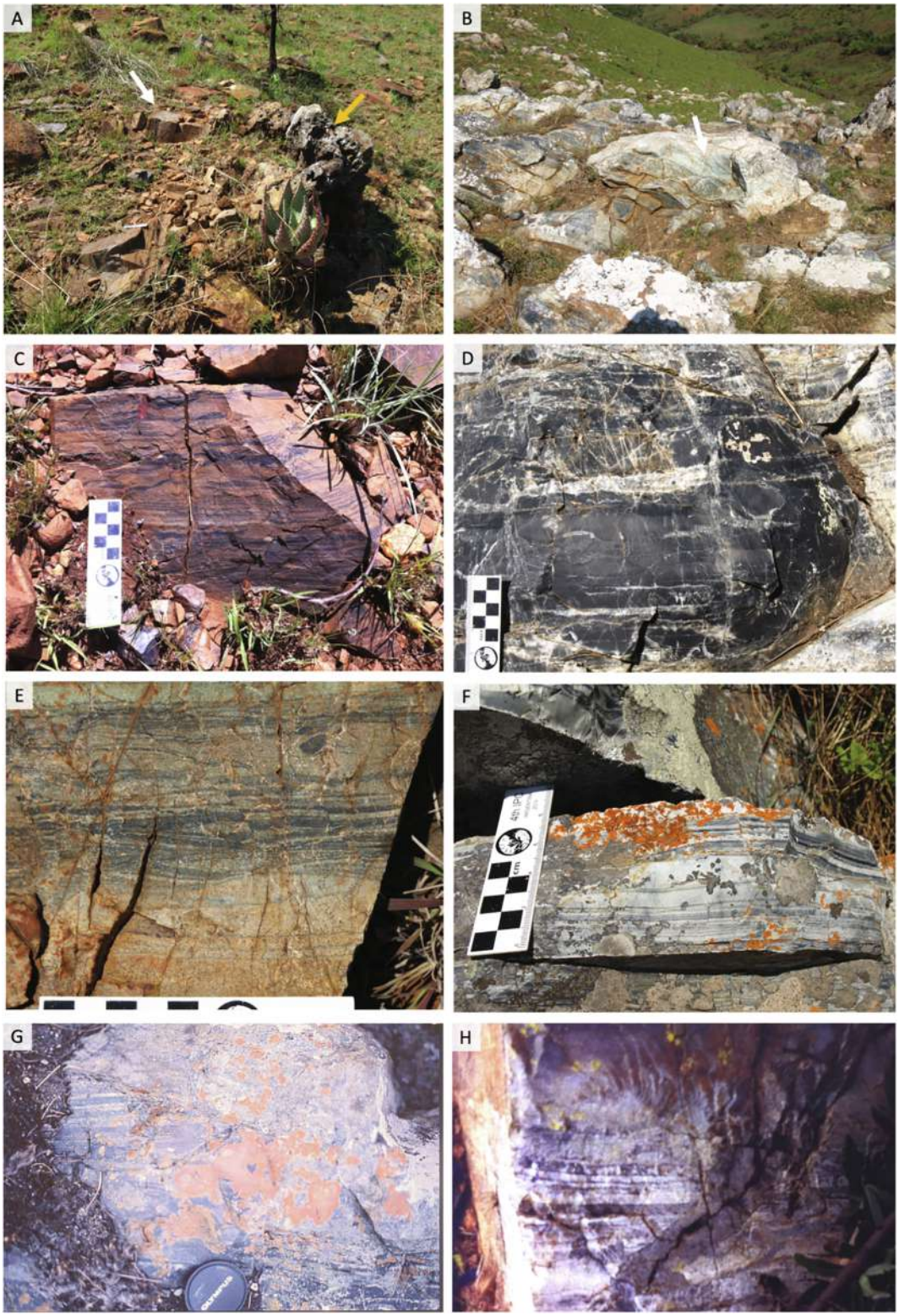

Fig. 3. Field and outcrop photographs from sampling localities. **A**) Field photograph of the Middle Marker horizon (north of Tjakastad, Mpumalanga province, South Africa) showing laminated cherts (white arrow) overlying basalt (orange arrow). **B**) Field photograph of the Josefsdal Chert (between Ekulindeni, Mpumalanga province, South Africa, and Bulembu, Hhohho region, Eswatini), showing laminated green-grey cherts (white arrow). **C**) Outcrop photograph of rippled, laminated, fine-grained silicified siltstone from the Middle Marker horizon, containing carbonaceous microbial laminations (sample 07SA23). **D**) Outcrop photograph of faintly-laminated carbon-rich chemical chert from the Josefsdal Chert (sample 99SA07). **E**) Detail of laminated chert from the Middle Marker horizon. **F**) Detail of grey-green laminated chert from the Josefsdal Chert. **G**) Outcrop photograph of black and white laminated chert from Hooggenoeg Formation Chert H5c (sample 03SA15). Lens cap for scale. **H**) Outcrop photograph of black and white laminated chert from the Footbridge Chert (samples 03SA09 and 03SA09′). Hammer shaft for scale. (For interpretation of the references to colour in this figure legend, the reader is referred to the web version of this article.)

2015). Although pervasive silicification may dilute REE + Y signatures, characteristic normalised patterns endure (Shields and Webb, 2004; Hofmann and Bolhar, 2007; Hofmann and Harris, 2008). Silica, either nucleating by sorption onto detrital particles in the watercolumn (Ledevin et al., 2014) or precipitating out of cooling, rock-buffered fluid resulting from the breakdown of olivine, pyroxene, feldspar and volcanic glass in sub-seafloor silicification zones, forms a rapidly crystallising ooze that entraps and co-locates detrital particles and carbonaceous material. The three-dimensional preservation of microbial mats (i.e., in volume) testifies to the fact that silicification began during mat growth (Hickman-Lewis et al., 2019). Thus, early and rapid silicification means that the REE + Y compositions of microbial horizons in ancient cherts reflect a snapshot of the ambient environments within which these ecosystems developed, flourished and were preserved.

Terrigenous clastic material may dominate REE + Y signals, and is often considered a '*contamination*', however, we do not advocate this terminology since the terrigenous fraction is a natural, *syn*-depositional sedimentary component of the biome and contributes to its elemental budget. Bio-available trace elements and REEs governed the metabolic landscape of the biome, and all co-occurring mineral phases contributed to this elemental budget. In brief, terrigenous signals should be considered important drivers of microbial-scale geochemistry, and not contaminants to the environment or rock sample.

Further to this, post-depositional processes including diagenesis and metamorphic events are comprehensively demonstrated to have negligible effects on REE + Y composition (e.g. Bau and Dulski, 1996; Bolhar et al., 2005; Gourcerol et al., 2016). This is sustained by the observation that specific REE + Y patterns coincide with expected palaeodepositional conditions, e.g., deposition in a shallow-water oxic or anoxic environments, after even upper greenschist facies metamorphism (Bau and Dulski, 1996). The REE + Y compositions of Archaean carbonaceous cherts may thus reflect the combinatorial influences of:

1) precipitation from anoxic marine water (Bau and Dulski, 1996; Van Kranendonk et al., 2003; Bolhar et al., 2004; Kamber and Webb, 2004);
2) hydrothermal fluids emanating from vent systems (Danielson et al., 1992; Kato and Nakamura, 2003; Bolhar et al., 2005; Allwood et al., 2010; Gourcerol et al., 2015);
3) additional non-marine influences, for instance lagoonal-lacustrine, riverine and local pore waters, some of which are enriched in REE + Y due to their siliciclastic fraction (Hoyle et al., 1984; Elderfield et al., 1990; Kato and Nakamura, 2003; Kamber et al., 2004; Bolhar and Van Kranendonk, 2007);
4) chemical inheritance after replacement of the protolith (Hanor and Duchac, 1990; Hofmann et al., 2013); and
5) complexation by organic molecules, such as carboxylate and phosphate groups in cell walls and extracellular polymeric substances (Takahashi et al., 2005; Censi et al., 2013; Freslon et al., 2014). In geological samples, normalisation to remove natural variations in REE + Y and allow comparison with upper crustal reservoirs is performed for Archaean rocks using Mud from Queensland (MuQ; *cf.* Kamber et al., 2005), which represents a bimodal felsic and mafic input, i.e. the expected terrigenous input from greenstone belts into Archaean oceans. When MUQ-normalised, most Precambrian sedimentary deposits can be abstractly characterised by a REE + Y pattern of seawater modulated by hydrothermal and other influences (Bau and Dulski, 1996; Allwood et al., 2010; Gourcerol et al., 2015), exhibiting:

i. enrichment in heavy rare earth elements (HREE) relative to light rare earth elements (LREE), and therefore low $(Pr/Yb)_{MUQ}$ signifying marine influence;
ii. super-chondritic Y/Ho ratios (Y/Ho ≥ 27) signifying marine influence;
iii. well-developed negative Ce anomalies if oxidation of Ce^{3+} to Ce^{4+} occurs in the water column;
iv. variably positive Eu anomalies reflecting hydrothermal contributions; herein, Eu anomalies will not be considered as signifying hydrothermal activity unless they exceed 1.2, since such values can also arise from enrichment within feldspars in tonalite-tronjhemite-granodiorite suites (Kerrich et al., 2013);
v. positive Y, La, Gd and Lu anomalies linked to marine input;
vi. the flattening of normalised patterns *via* enrichment in LREEs resulting signifying terrigenous, riverine influences (continental runoff), which are rapidly altered to typical seawater patterns during estuarine interaction with marine waters (Hoyle et al., 1984; Elderfield et al., 1990; Bolhar and Van Kranendonk, 2007; Sugahara et al., 2010); and
vii. MREE and especially HREE enrichment (Sm, Tm, Yb and Lu) resulting from inner sphere complexes during adsorption onto microbial cellular material (Takahashi et al., 2005; Censi et al., 2013; Freslon et al., 2014).

The concentration of REE + Y in sediments is a function of sourcewgeology but qualitatively similar sources can exhibit very different REE + Y concentrations with similar anomaly characteristics, e.g., the riverine-derived REE + Y chemistries in Elderfield et al. (1990) and Freslon et al. (2014) show markedly different REE + Y concentrations, however, the trend of the normalised pattern and its anomaly characteristics are comparable. This is because, unlike concentrations, anomalies (e.g., in La, Ce, Eu, Gd, Y and Lu) reflect complexation phenomena unique to specific hydrospheric chemistry. When normalised to their source rocks, marine deposits generally exhibit a non-smooth abundance pattern with relatively low $(Pr/Yb)_{MUQ}$ (Bau and Dulski, 1996; Bau, 1999). The REE + Y patterns of Archaean and modern sediments are similar (Bau and Dulski, 1996; Shields and Webb, 2004; Thurston et al., 2012), although the Archaean oceans carry the signal of greater hydrothermal fluid influence (Danielson et al., 1992; Klinkhammer et al., 1994; Wheat et al., 2002), accounted for by the positive Eu anomaly in almost all previously reported hydrogenous REE + Y patterns from Archaean sediments. Anoxic Archaean conditions further negate the redox effects culminating in negative Ce anomalies (De Carlo and Green, 2002; Kamber et al., 2004; Allwood et al., 2010; Tostevin et al., 2016), although the magnitude of Ce/Ce^*_{MUQ} can be altered even by small-scale changes in pH and redox (De Carlo and Green, 2002; Gourcerol et al., 2016), for example in restricted settings (Gourcerol et al., 2016). Artefact Ce anomalies are, however, unlikely in Archaean hydrogenous deposits due to the low levels of free O_2 present in the atmosphere (Bolhar and Van Kranendonk, 2007). Consequently, while a negative Ce anomaly indicates that dissolved O_2 was present in sufficient abundance to promote oxidation of Ce^{3+}, the absence of a Ce anomaly may be equivocal.

Riverine waters have significant impacts on REE + Y patterns since they are enriched in lanthanides relative to seawater (Elderfield et al., 1990; Klinkhammer et al., 1994; Alibo and Nozaki, 1999; Tostevin et al., 2016). This mathematically results in the suppression of anomalies due to near-uniform increases of up to several orders of magnitude in especially LREE and MREE concentrations. Freslon et al. (2014) also suggested that the REE + Y patterns of organic-rich sediments could be primarily controlled by biogeochemical processes relating to sedimentary organic matter and not by source composition. REE + Y patterns for organic matter presented by Takahashi et al. (2005) and Freslon et al. (2014) show strong MREE (Sm-Tb) and HREE (Tm-Lu) enrichment that may signify this effect.

As a final note, we have elected not to consider Gd anomalies in our discussion due to the low concentrations of Gd, Eu and Tb in the analytes studied, which may result in the inaccurate calculation of anomalies (Alibo and Nozaki, 1999; Kamber et al., 2004; Gourcerol et al., 2015, 2016).

Table 1
Sample details indicating sedimentary and textural characteristics, modes of accumulation of carbonaceous materials, and the scales of analyses performed (bulk ICP-MS or *in situ* laser ablation (LA) ICP-MS.

	Sample number	Description	Carbonaceous particles	Microbial mats	ICP-MS	LA ICP-MS
Middle Marker horizon	03SA01	Silicified sand-grade volcaniclastics			X	
	04SA14	Laminated clastic black-white chert	X	X	X	
	07SA21	Laminated black-white–grey chert with microbial fabrics	X	X	X	
	07SA22	Massive clotted carbonaceous chert	X		X	X
	07SA23	Laminated black-white–grey chert with microbial fabrics	X	X		X
	07SA25	Massive clotted carbonaceous chert	X			X
Hooggenoeg Fm.H5c chert	01SA09	Black-white–grey chert			X	
	01SA56	Silicified sand-grade volcaniclastics			X	
	03SA04	Black-white–grey chert	X			X
	03SA15	Laminated black-white–grey chert with microbial fabrics	X	X		X
	03SA16	Black-white–grey chert	X		X	
	07SA28	Black-white–grey silicified sediment			X	
Footbridge Chert	96SA02	Silicified sand-grade volcaniclastics			X	
	03SA09	Laminated black-white–grey chert with microbial fabrics	X	X		X
	03SA09′	Massive clotted carbonaceous chert	X			X
	12SA49	Black-white–grey chert	X		X	
	12SA50	Black-white–grey chert	X		X	
Josefsdal Chert	99SA07	Finely laminated clotted carbonaceous chert				X
	12SA01	Green-grey silicified volcaniclastics			X	
	12SA06	Black-white–grey chert			X	
	12SA10	Finely laminated black-white–grey chert			X	
	12SA13	Laminated black-green chert			X	
	12SA16	Laminated black-white–grey chert with microbial fabrics	X	X	X	
	12SA18	Laminated black-white–grey chert with microbial fabrics	X	X		X
	12SA20	Massive black chert			X	
	12SA22	Laminated black-white–grey chert with ferruginous layers			X	
	12SA29	Massive black chert			X	
	12SA32	Laminated black-white chert	X		X	
	12SA34	Laminated black-white chert	X		X	
	12SA36	Laminated black-green chert with microbial fabrics	X	X		X
	12SA37	Laminated black-white chert			X	
	14SA01	Massive black chert	X		X	
	14SA04	Black-white–grey chert with ferruginous zones	X		X	

2. Materials and methods

Samples were collected during multiple fieldwork campaigns to the Barberton greenstone belt between 1999 and 2014, and all may be readily relocated by their co-ordinates in Global Positioning Systems (G.P.S.). Table 1 summarises the studied samples by horizon and details their principal characteristics. All samples are stored in the CNRS Orléans Lithothèque.

2.1. Geological setting and petrography of microbial mats

Optical photomicrographs were acquired using an Olympus BX-51 equipped with a CCD camera (CNRS CBM, Orléans). Stratigraphic and petrographic descriptions of the context of the microbial horizons studied herein are as follows.

2.1.1. Middle Marker H1 (~3.472 Ga)

Bulk ICP-MS: The Middle Marker horizon is a thin chert unit (Fig. 3A), at the base of the Hooggenoeg Formation, charting the deposition of a shallow, wave- and current-influenced prograding volcanic cone within a semi-restricted basin (Lanier and Lowe, 1982; Paris et al., 1985; Hickman-Lewis et al., 2018a). Sediments vary between coarse-grained volcaniclastic sandstones, laminated volcaniclastic sandstones and siltstones and massive, clotted carbonaceous chert, with localised carbonate (calcite-dolomite) sedimentation (Fig. 3C, E; Tankard et al., 1982; Hickman-Lewis et al., 2018a). Previous bulk characterisation of major and trace element geochemistry suggests inputs from mafic and felsic volcaniclastic inputs (Hofmann et al., 2013; Hickman-Lewis et al., 2018a). Five representative samples were studied in bulk: three black-white–grey-green banded cherts (04SA14, 07SA21 and 07SA23) and two massive cherts with a significant volcaniclastic component (03SA01 and 07SA22).

LA ICP-MS: The Middle Marker horizon preserves an assemblage of morphologically diverse microbial mats, preserved in laminated volcaniclastic sandstones and siltstones that deposited in the photic zone, hence their interpretation as anoxygenic photosynthesisers (Hickman-Lewis et al., 2018a, 2019). These multi-laminar, crinkly-wavy, micro-tufted, carbonaceous laminations are common features mantling primary sedimentary structures. Using LA ICP-MS, a representative multi-laminar, micro-tufted suite of mats (ca. 1 cm thick; sample 07SA23) from laminated volcaniclastic sandstones (Fig. 2A) were studied. Three-dimensional reconstructions of these mats show that they exhibit micro-tufted topographies and trap and bind particles (Hickman-Lewis et al., 2019). Two samples of massive carbonaceous black chert (07SA22 and 07SA25), were also studied in order to understand normal, local-scale geochemical conditions between mat growth (Fig. 2B, S1).

2.1.2. Hooggenoeg chert H5c (ca. 3.47–3.45 Ga)

Bulk ICP-MS: The Hooggenoeg Chert H5 member is a unit of ultramafic and mafic volcanics, overlain by silicified volcaniclastic sedimentary rocks and laminated, black-grey carbonaceous chert with botryoidal stratiform veins (H5c; Fig. 2G) (Lowe and Byerly, 1999; Hofmann, 2011). Chert veins crosscutting silicified volcanic rocks immediately below the chert horizons throughout the Hooggenoeg Formation are interpreted as the result of shallow hydrothermal convection of seawater (Hofmann and Bolhar, 2007; Hofmann, 2011). Early silicification in the laminated chert is indicated by a planar contact with the overlying conglomerate (Hofmann and Bolhar, 2007). Two samples each of black and white laminated cherts (01SA56 and 07S28) and massive black cherts (01SA09 and 03SA16) were studied in bulk.

LA ICP-MS: Biosignatures from Hooggenoeg chert H5c include filamentous microfossils and carbonaceous laminations (Walsh, 1992;

Walsh and Lowe, 1999; Hickman-Lewis et al., 2018b). The morphological similarity of the latter to modern and fossil microbial mats, together with trapped and bound particles, and roll-up and anastomosing structures providing evidence of *in vivo* plasticity, are convincing evidence for their biogenetico. The microbial mats studied herein using LA ICP-MS (from sample 03SA15) have flat-laminated morphologies (Fig. 2C), similar to those described in Walsh (1992) and Walsh and Lowe (1999). A further sample of adjacent massive carbonaceous black chert (sample 03SA04; Fig. 2D, S2) was analysed to understand normal, local-scale geochemical environments between mat growth.

2.1.3. Footbridge chert K3c (3.334 Ga)

Bulk ICP-MS: The Footbridge Chert is a sequence of laminated and massive cherts (Fig. 3H) deposited in alternately shallow- (Westall et al., 2001) and deep-water (i.e., below storm wave base; Lowe and Byerly, 1999) conditions. Much of this chert is underlain by silicified pillow basalt with cross-cutting and stratiform botryoidal veins that continue upward through the laminated chert (Hofmann and Bolhar, 2007). Two laminated shallow-water cherts (12SA49 and 12SA50) and one sample of silicified volcaniclastic green-grey chert (96SA02), reflecting the dominant mineralogies of this sequence, were studied in bulk.

LA ICP-MS: Thin, carbonaceous laminations can be identified in the shallow-waterhorizons of some banded cherts, although these structures have never before been described. Their similarity to known microbial mats from the Archaean makes their biogenic interpretation plausible and unsurprising. Within the studied samples of black and white laminated chert (03SA09), carbonaceous laminations forming layers of several hundred microns' thickness drape over and anastomose around large, rounded carbonaceous grains and over layers comprising detrital deposits of volcaniclastic particles (Fig. 2E). These laminations form 'eyelet' structures around enclosed particles bearing considerable resemblance to alpha-type laminations from the Buck Reef Chert (Tice and Lowe, 2006a,b). Furthermore, roll-up and rip-up structures often occur at the surfaces of laminations, denoting plasticity *in vivo*. Above one of the studied mat horizons, a particularly well-preserved, frayed, torn-up mat chip can be linked to the eroded surface morphology of the underlying horizon (Fig. 2E, S3). A very high degree of volumetric preservation is recorded within each microbial horizon, suggesting almost immediate seafloor silicification. A sequence of these exceptionally preserved mats are preserved in sample 03SA09; a transect through two of these mats was conducted using LA ICP-MS. A sample of massive chert from immediately below these horizons (03SA09′) was also studied to constrain normal, local-scale chemistries between mat growth (Fig. 2F, S3C).

2.1.4. Josefsdal Chert ~ K3c (ca. 3.33 Ga)

ICP-MS: The Josefsdal Chert is an 8–30 m thick sequence of volcaniclastic sandstones, carbonaceous and ferruginous chert with variable hydrothermal influence, and biogenic sediments (Fig. 3B, D, F), all of which deposited in a shallow basin atop basaltic pillow lavas (Westall et al., 2015). The sequence includes localised chemical cherts that precipitated as a silica-rich ooze (*cf*. Ledevin et al., 2014). The depositional basin appears to have been protected, indicated by a general lack of large-scale sedimentary bedforms indicative of open sea conditions and the parallel-laminated structure of most microbial mat horizons. The samples studied herein include finely laminated chemical chert strata (Fig. 2H, 3D, S4) and shallow-water,laminated, organic carbon-bearing sediments from upper shoreface settings, including mixed detrital and microbial carbonaceous material (Fig. 2G, S4), e.g. carbonaceous laminations. Bulk analyses were conducted in a number of black-grey-white banded cherts and massive cherts (see Table 1).

LA ICP-MS: Within the Josefsdal Chert, thin microbial biofilms occur in both banded sedimentary and chemical cherts, and bear much morphological similarity to those previously described in the Hooggenoeg Formation, trapping and binding grains and mantling large carbonaceous particles (Westall et al., 2011, 2015). Putative microfossils occur in the same horizons (Westall et al., 2001, 2015). Previous high-resolution geochemical analyses of one such biofilm suggest that it consisted of a consortium of phototrophic organisms and sulphate-reducing bacteria (Westall et al., 2011). LA ICP-MS 'biome'-scale transect analyses were conducted across microbial horizons in two banded cherts (12SA18 and 12SA36) and one massive chert (99SA07).

2.2. Geochemistry of microbial mats

2.2.1. Bulk ICP-OES and ICP-MS

Inductively coupled plasma optical emission spectrometry (ICP-OES) and mass spectrometry (ICP-MS) analyses were conducted at the Centre de Recherches Pétrographiques et Géochimiques (CRPG), Nancy, France, using Thermo Fisher ICap 6500 and Agilent 7700X instruments. Analysed powders were sub-sampled from chips of the original hand samples demonstrably free of obvious alteration and secondary veining. We focussed on both characteristic chert matrices without microbial mat fabrics – i.e., representative of these horizons in bulk ('regional' scale) – and those with microbial horizons and their immediate environs ('local' scale), thereby enabling direct comparison with LA ICP-MS measurements ('biome' scale) (Fig. 1). Results of bulk ICP-OES major element analyses are shown in Fig. 4. Results of bulk ICP-MS analyses are shown as extended trace element diagrams in Fig. 5, as REE + Y curves in Fig. 6, and as mixing line diagrams (see Section 2.3.) in Fig. 7.

2.2.2. In situ laser ablation ICP-MS

For laser ablation (LA) ICP-MS, thin sections of between 60 μm and 100 μm thickness were produced from complementary samples in which regions of interest (ROIs) in chert were identified using high-magnification optical microscopy. ROIs were selected to be clean and free from phases that might contaminate the primary REE + Y signature (see Gourcerol et al., 2015), for example, diagenetic oxides and sulphides, and also secondary features including veining, destructive recrystallisation and oxidative weathering of weaknesses and fractures. To assure the validity of our conclusions regarding the co-evolution of life and its environment ('local' and 'biome' scale), REE + Y compositions must stem only from the interaction of primary inputs, such as contemporaneous terrigenous material, with aqueous reservoirs. Due to the rapidity of silicification outlined above, primary phases should be considered important in defining the elemental budget and geochemistry of their horizon.

Within samples hosting microbial mats, multiple transects of laser ablation point analyses were taken through these horizons (Fig. 1B) in order to capture fine-scale palaeoenvironmental fluctuations during the short timescales of microbial colonisation ('biome' scale). In order to specifically address the palaeodepositional setting of microbial mats, we pre-scanned the studied areas with high-resolution optical microscopy in order to be certain to analyse *exclusively chert domains* within mat layers, and not the organic matter itself, which usually occurs as a readily identifiable interstital phase (e.g. De Gregorio and Sharp, 2006). High rates of MREE and HREE scavenging by microbial and sedimentary organic matter can dominate the REE + Y pattern (Takahashi et al., 2005; Censi et al., 2013; Freslon et al., 2014). Avoiding carbonaceous materials ensures that laser ablation analyses sample exclusively ambient aqueous reservoirs with minimal to zero organic influence.

Data were acquired using a XSeries II ICP-MS (Thermo Fischer Scientific) coupled to a 213 nm Nd:YAG laser ablation system (New Wave Research) housed at the Centro Interdipartimentale Grandi Strumenti (CIGS), Università di Modena e Reggio Emilia, Italy. Helium was used as the carrier gas to transport ablated material from the LA sample chamber to the mass spectrometer torch. Standard Reference Materials NIST 610, NIST 612 and NIST 614 (National Institute of Standards and Technology) were used to perform external calibration

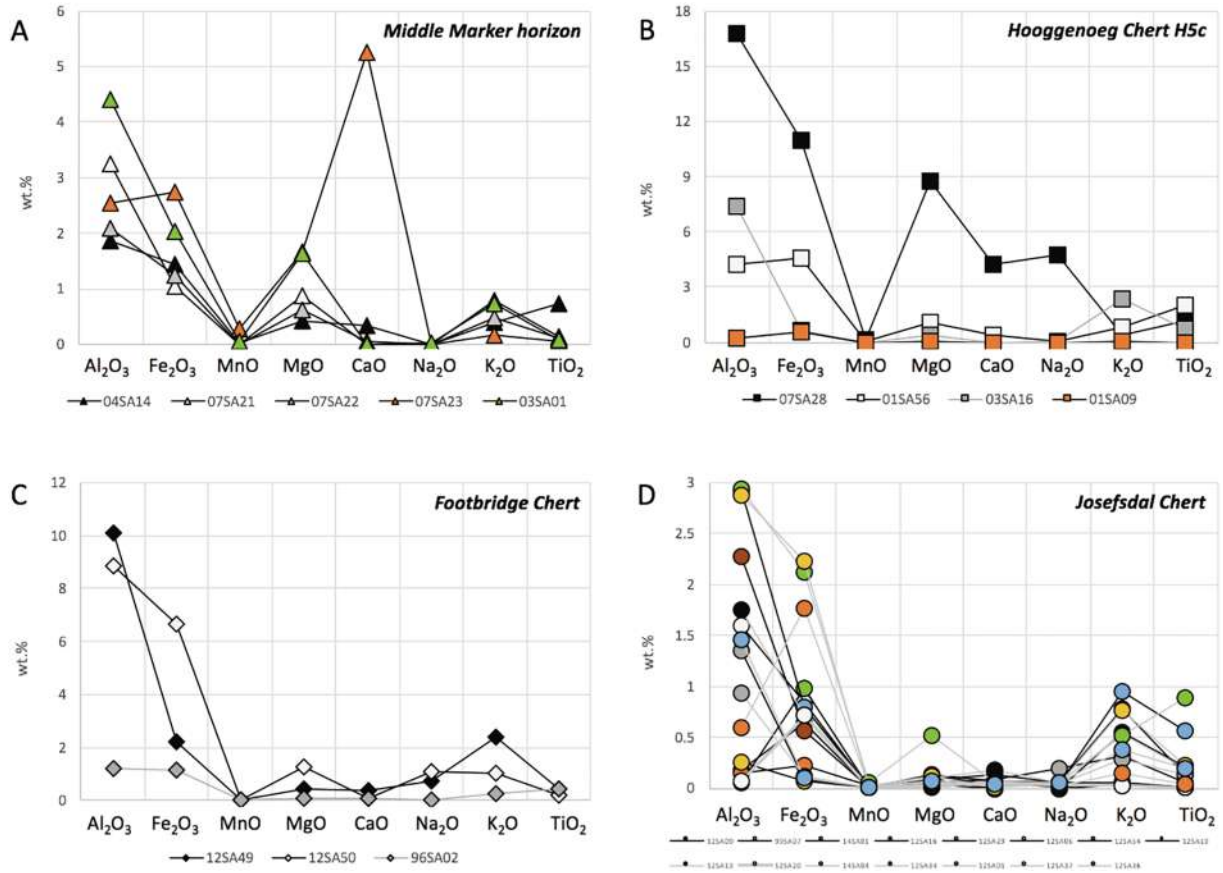

Fig. 4. ICP-OES analyses of major element concentrations in bulk samples. **A**) Middle Marker horizon. **B**) Hooggenoeg Chert H5c. **C**) Footbridge Chert. **D**) Josefsdal Chert. This colour code is specific to bulk samples and used only for this figure and Fig. S5. The rest of each sample is composed of the matrix phase SiO_2 (see Fig. 5).

and mass spectrometer tuning, and were measured during each analysis with equivalent spot size, frequency, duration and laser intensity as the samples (Table 2). Instrumental performance was optimised daily using NIST 612 as reference material in order to obtain maximum signal intensity. Mass spectrometer parameters were tuned for the maximum signals of ^{139}La, ^{232}Th and ^{238}U while ablating a line on NIST 612 with the following parameters: line width = 100 µm, repetition rate = 10 Hz, laser output = 100%.

To maximise the quality of analytical data, several laser parameters, such as ablated area, beam intensity, frequency and ablation and blank duration, were systematically varied in order to evaluate their effects on signal quality. Several preliminary tests were performed on a representative sample (07SA23) in order to determine the parameters used for analyses. During preliminary tests, it was also demonstrated that pre-ablation was necessary to remove possible contaminants from the sample surface before data acquisition. The signal acquired during each analysis involved three steps: pre-ablation, blank acquisition and ablation. Signals acquired during pre-ablation were not used for calculation. After pre-ablation, the laser was turned off and a blank signal (background) was acquired. This step was immediately followed by sample ablation to obtain a time-dependent signal. The blank was used to correct for the background: once appropriate time-resolved sections were chosen for the blank and the sample, the average background signal intensity was subtracted from the average sample signal intensities. A summary of the LA parameters used during the experimental sessions is presented in Table 2.

Concentrations of the analytes of interest were obtained by comparison with the external calibration curve (NIST 610, 612 and 614). Quantitative data were obtained for the following: ^{7}Li, ^{9}Be, ^{23}Na, ^{26}Mg, ^{27}Al, ^{28}Si, ^{31}P, ^{39}K, ^{44}Ca, ^{45}Sc, ^{47}Ti, ^{51}V, ^{52}Cr, ^{55}Mn, ^{56}Fe, ^{59}Co, ^{60}Ni, ^{63}Cu, ^{66}Zn, ^{69}Ga, ^{75}As, ^{85}Rb, ^{88}Sr, ^{89}Y, ^{90}Zr, ^{93}Nb, ^{95}Mo, ^{107}Ag, ^{109}Ag, ^{111}Cd, ^{115}In, ^{118}Sn, ^{123}Sb, ^{133}Cs, ^{137}Ba, ^{139}La, ^{140}Ce, ^{141}Pr, ^{146}Nd, ^{147}Sm, ^{153}Eu, ^{157}Gd, ^{159}Tb, ^{163}Dy, ^{165}Ho, ^{166}Er, ^{169}Tm, ^{172}Yb, ^{175}Lu, ^{178}Hf, ^{181}Ta, ^{182}W, ^{197}Au, ^{205}Tl, ^{208}Pb, ^{232}Th, ^{238}U. At least three spots were acquired in each region of interest (see Supplementary Tables). The results of *in situ* laser ablation ICP-MS analyses are shown as REE + Y curves in Fig. 8, plotted against mixing lines in Fig. 9, and shown in terms of the changing chemistry through microbial mat transect analyses in Fig. 10.

Elemental anomalies relative to neighbouring and near-neighbouring elements in ICP-MS and LA ICP-MS plots were calculated according to the methods presented in Lawrence and Kamber (2006) and Lawrence et al. (2006) as follows:

$$La/La^{*}_{MuQ} = La_{MuQ}/(Pr^{*}_{MuQ}(Pr_{MuQ}/Nd_{MuQ})^{2})$$

$$Ce/Ce^{*}_{MuQ} = Ce_{MuQ}/(Pr^{*}_{MuQ}(Pr_{MuQ}/Nd_{MuQ})$$

$$Pr/Pr^{*}_{MuQ} = Pr_{MuQ}/(0.5Ce_{MuQ} + 0.5Nd_{MuQ})$$

$$Eu/Eu^{*}_{MuQ} = Eu_{MuQ}/(Sm^{2}_{MuQ} \times Tb_{MuQ})^{1/3}$$

$$Y/Y^{*}_{MuQ} = Y_{MuQ}/(0.5Er_{MuQ} \times 0.5Ho_{MuQ})$$

2.3. Mixing line diagrams

The respective influences of high-temperature (> 250 °C) hydrothermal fluids and detrital inputs were assessed using calculated binary mixing lines (Figs. 7, 9). End-members reflecting seawater, hydrothermal fluid and detrital terrigenous influence were selected, respectively, as follows after Gourcerol et al. (2016):

- modern seawater from the North Pacific (Alibo and Nozaki, 1999);w

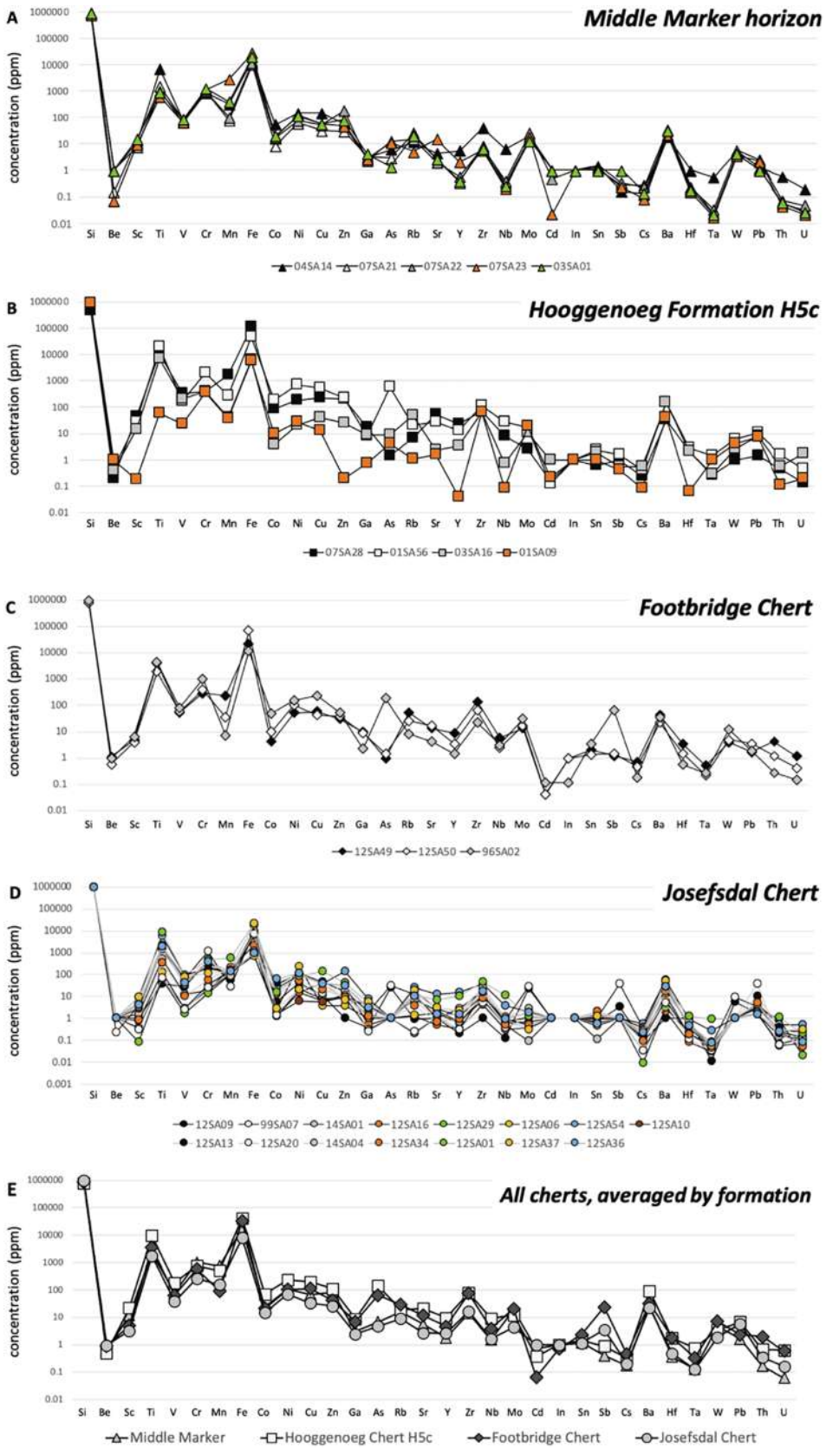

Fig. 5. Extended ICP-MS major and trace element compositions of samples. **A**) Middle Marker horizon. **B**) Hooggenoeg Chert H5c. **C**) Footbridge Chert. **D**) Josefsdal Chert. **E**) Averaged compositions from the four studied formations illustrating their similar chemical trends.

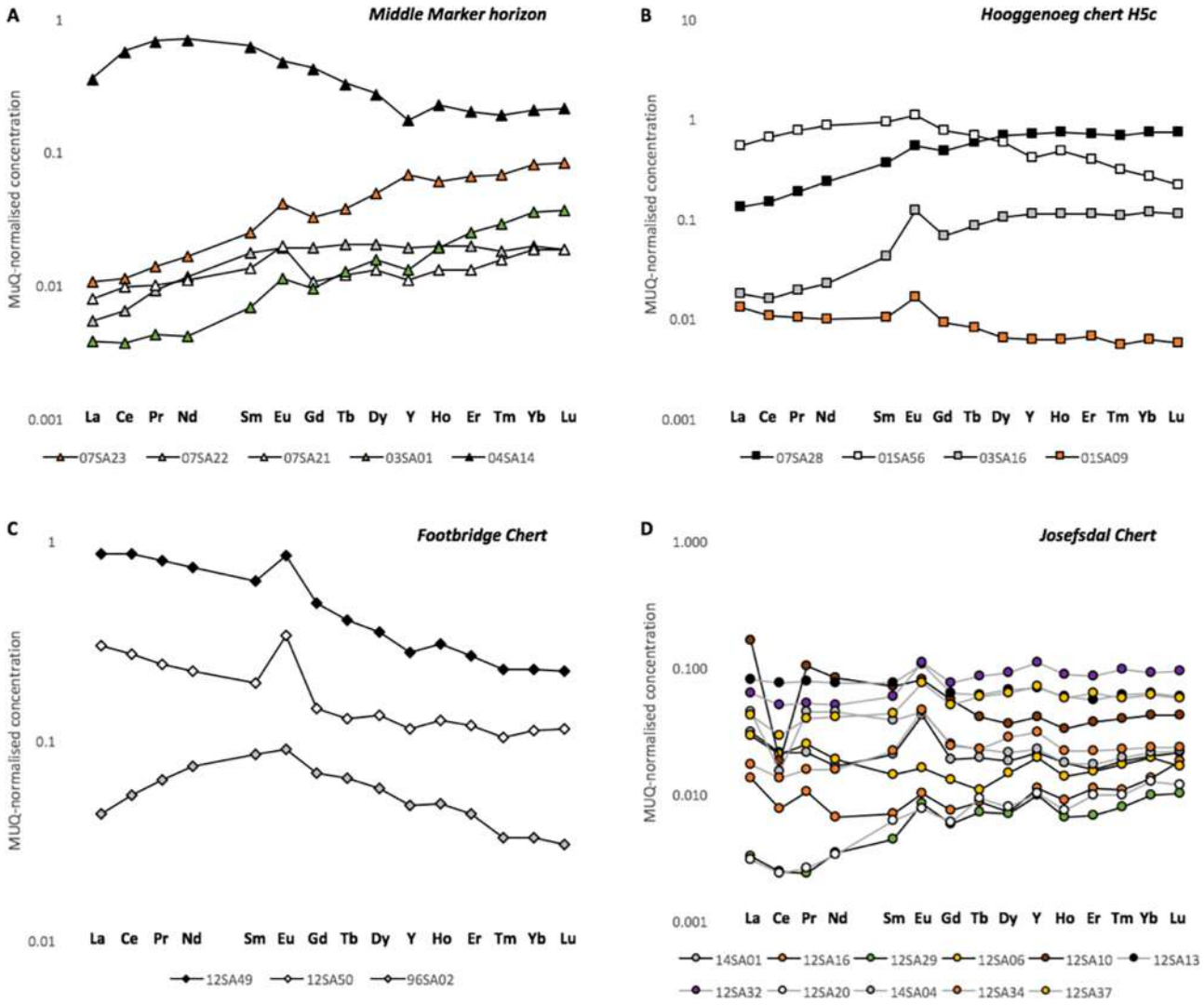

Fig. 6. MuQ-normalised bulk ICP-MS measurements of REE + Y in the four studied units. **A**) Middle Marker horizon samples, exhibiting patterns typical of Archaean hydrogenous sedimentation, with the exception of 04SA14, whose geochemistry may have been altered by post-diagenetic effects (data partly from Hickman-Lewis et al., 2018a). **B**) Hooggenoeg Formation chert H5c samples: two samples (07SA28 and 03SA16) exhibit typical patterns of Archaean seawater, whereas another two (01SA56 and 01SA09) show inverse patterns in which LREE are enriched relative to HREE. **C**) Footbridge Chert samples: two samples, 12SA49 and 12SA50, show LREE enrichment over HREE with characteristics of Archaean seawater. Sample 96SA02 exhibits MREE enrichment superimposed on a similar trend. **D**) Josefsdal Chert samples, generally exhibiting the typical patterns of Archaean hydrogenous sedimentation with elevated LREE concentration (data partly from Westall et al., 2015).

- hydrothermal chert from a banded iron formation of the Abitibi greenstone belt, Canada, (Thurston et al., 2012) characterised by a very strong Eu anomaly (Eu/Eu^*_{MUQ} = 30.01); and
- Mud from Queensland (MuQ), i.e., bimodal mafic-felsic terrigenous input (Kamber et al., 2004).

Eu/Sm *versus* Sm/Yb mixing lines were used to quantitatively determine the influence of hydrothermal activity on each sample. Seawater from the North Pacific (Alibo and Nozaki, 1999) was used as the marine end-member. Gourcerol et al. (2016) determined that a brecciated chert sample from Thurston et al. (2012) with a large Eu anomaly (Eu^*/Eu_{MUQ} = 30.01) provides an accurate model for Archaean hydrothermal effluent, since pre-Proterozoic hydrothermal venting regions were characterised by fluid mixing with an inverse pH gradient (alkali to acid) when compared to modern hydrothermal systems (Shibuya et al., 2010). Consequently, the Eu/Sm and Sm/Yb ratios, which are respectively a quantitative measurement of the strength of the Eu anomaly and a measure of the flatness of the REE + Y pattern, may be used to quantify the influence of high-temperature (> 250 °C) hydrothermal fluids, which are characterised by a flat REE + Y pattern devoid of all except the Eu anomaly. Most Archaean samples plot either on or above the mixing line calculated from the seawater and hydrothermal end-members since the Sm/Yb ratio is sensitive to high-pressure residual metamorphic phases, Points plotting far from the mixing line are not pristine and will not be considered in our discussion.

$(Pr/Nd)_{MUQ}$ *versus* Y/Ho ratios, which are respectively measurements of the flatness of the REE + Y pattern and the chondritic values of the fluid, were used to qualitatively assess detrital terrigenous input during chert deposition, since terrigenous input is characterised by flat REE + Y patterns and chondritic Y/Ho ratios. A conservative mixing line was calculated using seawater from the North Pacific (Alibo and Nozaki, 1999) and the MuQ composite (Kamber et al., 2004) as end-members. Note that the percentage values in these diagrams should be considered as the relative influence of the end members rather than a quantitative measure. Further detail on the rationale for the construction of these mixing lines is presented in Gourcerol et al. (2016).

Together, these two mixing plots indicate, using independent elemental ratios, marine *versus* hydrothermal and marine *versus* terrestrial

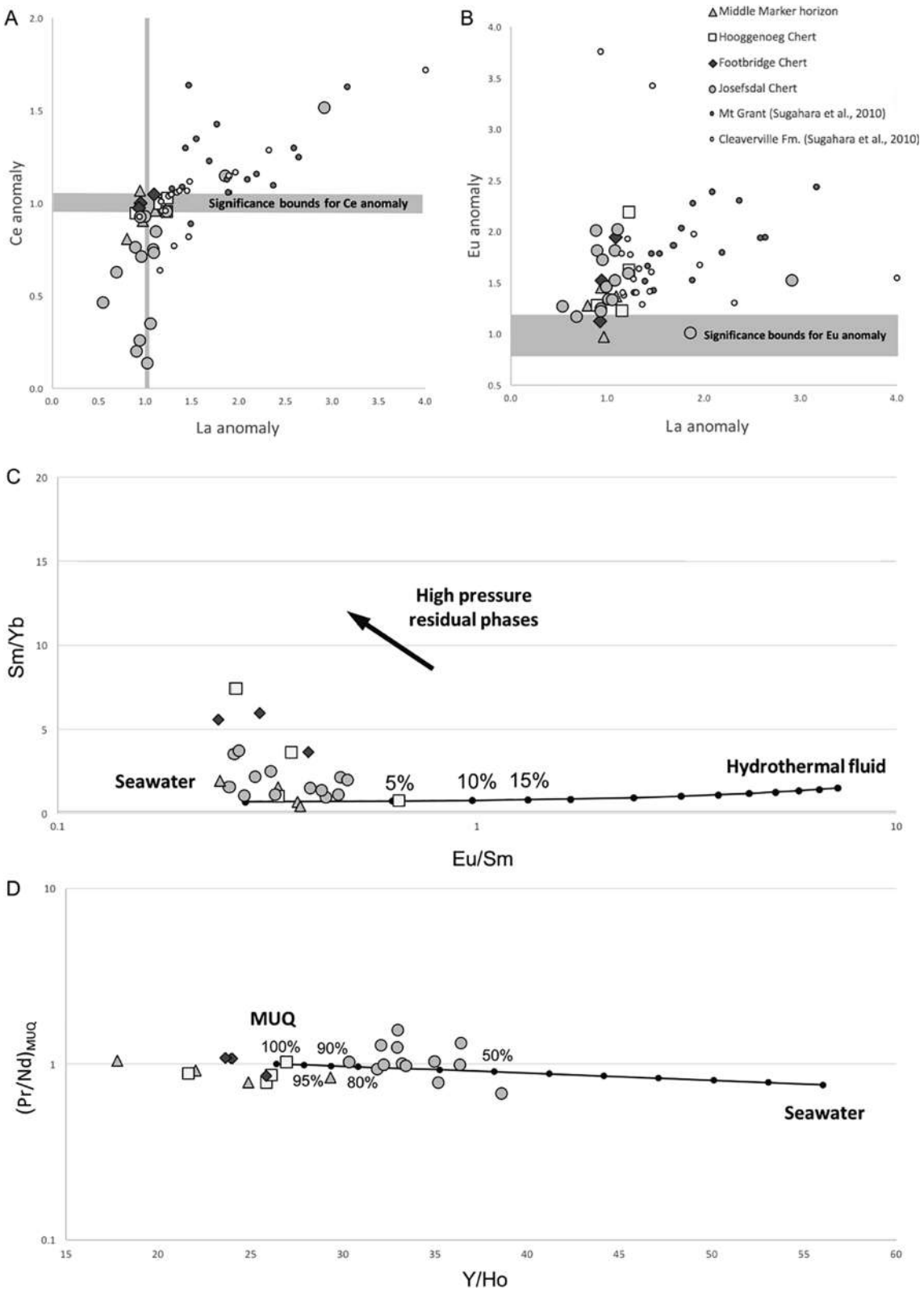

Fig. 7. Bulk ICP-MS analyses compared, where relevant, to those of other fossiliferous, carbonaceous cherts (from Sugahara et al., 2010). **A**) La anomaly *versus* Ce anomaly. Vertical grey line denotes $La/La^*_{MuQ} = 1$, i.e. no significant La anomaly. Horizontal grey zone denotes the significance bounds of the Ce anomaly, i.e. Ce/Ce^*_{MuQ} between 0.95 and 1.05 are deemed not significant (after Bau and Dulski, 1996). **B**) La/La^*_{MuQ} *versus* Eu/Eu^*_{MuQ}, the former diagnostic of marine hydrogenous depositions, the latter denoting the contribution of hydrothermal fluids. Horizontal grey line denotes the significance bounds of the Eu anomaly, i.e. Eu/Eu^*_{MuQ} is only considered significant if > 1.2 (Kerrich et al., 2013). **C**) Eu/Sm *versus* Sm/Yb mixing line plot showing the quantitative contribution of hydrothermal fluid. **D**) Y/Ho *versus* $(Pr/Nd)_{MuQ}$ mixing line plot qualitatively assessing terrigenous (non-marine) influence. C-D are plotted after methods described in Gourcerol et al. (2016), outlined in the main text.

Table 2
Parameters used during laser ablation ICP-MS experiments.

Parameters	*Values*
Pre–ablation:	
Spot size (μm)	40/65 (depending on the size of the region of interest)
Frequency (Hz)	10
Duration (s)	5
Laser intensity (%)	25
Ablation:	
Spot size (μm)	40/65 (depending on the size of the region of interest)
Frequency (Hz)	20
Duration (s)	30
Laser intensity (%)	100
Total acquisition time (s)	150
Laser warm up (s)	25
Wash out (s)	30
He flowrate (mL/min)	600
Mass spectrometer dwell time per analyte (ms)	30

(i.e., non-marine) inputs. In the case of a significant non-marine input, one must consider the magnitude of the Eu anomaly in distinguishing whether the input is hydrothermal or riverine.

3. Results

3.1. Evaluation of contamination and metamorphism

Since even small quantities of clastic- or mineral-related input can affect the REE + Y signal of hydrogenous chert, we have followed the rigorous approaches of Bolhar and Van Kranendonk (2007), Sugahara et al. (2010) and Bolhar et al. (2015) to test that clastic or terrigenous components can be considered a *primary input*, and not *post-depositional contamination*, to the palaeoenvironment. For each formation, we tested multiple parameters (La, Eu, Ce and Y anomalies and Y/Ho ratios) against total REE + Y, Ti content, and against one another, as a proxy for contamination of the signal by overprinting clastic input or other hydrospheric and diagenetic influences. We found no systematic relationships between any two such parameters (Figs. S5–S6), ergo '*contamination*' does not affect the REE + Y signals reported (*cf.* Sugahara et al., 2010; Bolhar et al., 2015). Our REE + Y compositions are thus unequivocally primary. Since similar values are obtained for various parameters (e.g. anomalies) irrespective of the Ti content, fluid chemistry rather than clastic contamination is the dominant control on REE + Y composition (Bolhar et al., 2015) (see also Figs. S8–S10).

Post-Archaean trace element mobilisation by either system reactivation or metamorphism is not relevant to the final REE + Y signature since the units studied underwent only lower greenschist facies (< 350 °C, 2–3 kbar) or zeolite facies (< 300 °C, < 2–3 kbar) metamorphism, which is insufficient to significantly alter REE + Y signals and their interpretation (Bau and Dulski, 1996; Bau, 1999; Shields and Webb, 2004). Specifically, for the Onverwacht Formation studied herein, Xie et al. (1997), Tice et al. (2004) and Hickman-Lewis et al. (2020) estimated metamorphic temperatures generally within the chlorite zone (285–400 °C), likely centred around 285–320 °C, using chlorite and Raman geothermometry.

3.2. Bulk ICP-OES and ICP-MS

All studied cherts have low concentrations of major (Fig. 4) and trace (Fig. 5) elements, with the exception of Si, which represents the overwhelming majority of the samples (the matrix). Specifics of individual sample compositions are detailed in the following. All measured data are given in the Supplementary Tables.

3.2.1. Middle Marker horizon

Bulk ICP-OES of five samples from the Middle Marker horizon cherts show that they vary between 80.9% and 94.8% SiO_2 and contain relatively high Al_2O_3, Fe_2O_3, MgO and K_2O content; furthermore, one sample (07SA23) has high (5.26 wt%) CaO content (Fig. 4A), which is corroborated by XRD measurements estimating ≤ 9 wt% calcite (Fig. S5G), although the Ca-Mg rich mineralogy also indicates dolomite. Cr and Mn are present at high concentrations, whereas Cd, Ta, Pb, Th and U are present in exceptionally low quantities (Fig. 5A, E).

In bulk sample (ICP-MS results), MuQ-normalised REE + Y characteristics show an enrichment of HREEs over LREEs: La anomalies are negative to negligible (La/La^*_{MuQ} = 0.74–1.09), Ce anomalies are weakly negative (Ce/Ce^*_{MuQ} = 0.81–1.07; Fig. S7A), Eu anomalies are weakly positive (Eu/Eu^*_{MuQ} = 0.98–1.46), and Y anomalies are generally negative (Y/Y^*_{MuQ} = 0.58–1.07) (Fig. 6A and 7, Table 3). Pr-Ce anomaly systematics indicate that the Ce/Ce^*_{MuQ} is often a 'true' anomaly (Fig. S7; *cf.* Bau and Dulski, 1996). Y/Ho values are sub-chondritic to super-chondritic, ranging between 17.7 and 29.3 (Table 3, Fig. 7).

3.2.2. Hooggenoeg chert H5c

Four samples of Hooggenoeg chert were studied by bulk ICP-OES and ICP-MS, which show two divergent chemical trends. 07SA28 and 01SA56 have relatively high concentrations of most major elements, whereas 01SA09 and 03SA16 contain considerably lower concentrations (Fig. 4B). SiO_2 ranges between 85.4% and 95.4%, however, 07SA28 is notably poor in SiO_2 (47.8%), having instead particularly high Al_2O_3, MgO and K_2O, reflecting volcanogenic input and/or limited silicification. 01SA56 is also rich in Al_2O_3, Fe_2O_3, MgO and TiO_2. ICP-MS bulk analyses show no clear trends in trace element composition between samples. The average composition of the Hooggenoeg Formation samples shows that they have significantly higher concentrations of many transition metals relative to the other cherts, including Fe, Co, Ni, Cu and Zn, and are also rich in Sc, Ti, As, Sr, Y and Ba (Fig. 5B, E).

In bulk sample (ICP-MS results), MuQ-normalised REE + Y characteristics show either typical seawater patterns of HREE > LREE (07SA28 and 03SA16), similar to Middle Marker cherts, or flatter patterns with MREE enrichment (01SA56 and 01SA09) (Fig. 6B). Eu anomalies are positive (1.23–2.19) (Fig. 6B, 7, Table 3). Other anomalies include weakly positive La/La^*_{MuQ} (0.89–1.22) and negligible Ce/Ce^*_{MuQ} (0.95–1.03, i.e. no 'true' anomaly; Fig. 7), and slightly negative Y/Y^*_{MuQ} (0.91–0.99). Y/Ho ratios are sub-chondritic (21.5–26.9; Table 3, Fig. 7).

3.2.3. Footbridge chert

Three representative bulk samples were chosen from the Footbridge Chert: samples 12SA49 and 12SA50 – two silicified shallow-water volcaniclastic sediments – contain higher Al_2O_3 and Fe_2O_3 than most other samples, but lower SiO_2 content (77.4–80.4%) (Fig. 4). 96SA02 – a silicified volcanic rock representative of the regional environment (*cf.* Lowe and Byerly, 1999) – comprises 96.0% SiO_2 and has high concentrations of Ni, Cu, As, Sn and W (Fig. 5C).

In bulk sample (ICP-MS results), MuQ-normalised REE + Y characteristics are quite different to most other samples (Fig. 6C). In samples 12SA49 and 12SA50, LREEs are strongly enriched relative to HREEs, and the absolute concentrations of REE + Y are very high. In the third sample, 96SA02, strong enrichment is present in MREEs. La/La^*_{MuQ}, Ce/Ce^*_{MuQ} and Y/Y^*_{MuQ} are negligible (respectively, 0.93–1.09, 0.98–1.00 and 0.93–1.02), however, Eu/Eu^*_{MuQ} is positive but not significant (1.13) in 96SA02 and 1.53–1.95 in the shallow-water laminated sediments (Fig. 7A-B, Table 3). The three samples are characterised by sub-chondritic Y/Ho values, which range from 23.6 to 25.8 (Table 3; Fig. 7).

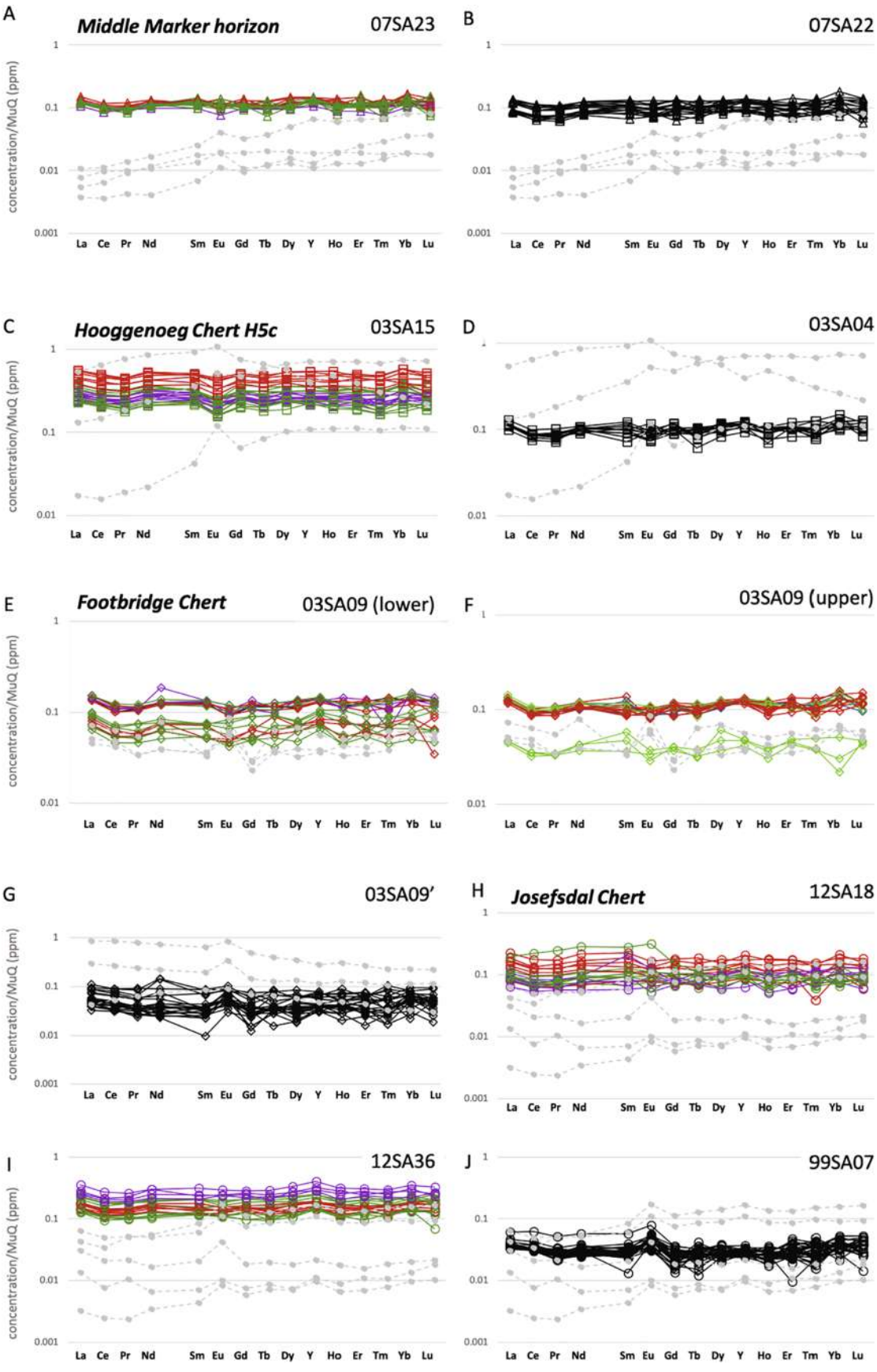

(caption on next page)

Fig. 8. *In situ* LA ICP-MS results (solid lines) compared with bulk ICP-MS (dashed grey lines, as in Fig. 6) showing MuQ-normalised REE + Y composition. Bulk ICP-MS results should be considered to represent prevailing local to regional palaeoenvironmental conditions, whereas *in situ* LA ICP-MS results indicate palaeoenvironmental conditions specific to the short timescales of microbial colonisation (biome-scale palaeoenvironments from transect analyses). **A-B**) Middle Marker horizon; **C-D**) Hooggenoeg Formation chert H5c; **E-G**) Footbridge Chert; **H-J**) Josefsdal Chert. All microbial horizons (red, green and purple lines) show elevated REE + Y content, and significantly higher LREE concentrations. Transects taken through microbial horizons in all cherts (i.e., coloured lines in A, C, E-F, H-I) show flat patterns often with negative Eu anomalies, suggesting elevated terrigenous influence and reduced hydrothermal influence. E-F show LA ICP-MS results from G as dotted grey lines to emphasise the absence of the Eu anomaly in microbial horizons. G uses bulk results from the Footbridge Chert as dotted grey lines. Coloured lines represent series of analyses in microbial horizons: red lines indicate analyses taken immediately below, green lines analyses within, and purple lines analyses immediately above microbial horizons. Black lines represent non-microbial horizons. (For interpretation of the references to colour in this figure legend, the reader is referred to the web version of this article.)

3.2.4. Josefsdal chert

The selected samples of Josefsdal Chert include intermixed volcanogenic and chemical sedimentary rocks, interpreted as hydrothermally influenced deposits, near-pure chert of proposed chemical precipitate origin, and shallow-water, laminated, organic carbon-bearing silicified volcanogenic sediments, in which microbial biofilms are preserved. All Josefsdal Chert samples have high SiO_2 contents between 85.5% and 99.9%. As with the other horizons, no clear between-sample trends in trace elements exist.

Bulk REE + Y compositions (ICP-MS results) are characteristic of the mixing of marine and hydrothermal waters, but are enriched in LREE relative to other cherts (Fig. 6D): La/La^*_{MuQ} ranges from weakly negative to strongly positive (0.68–2.90), Ce/Ce^*_{MuQ} spans a range from very negative to weakly positive (0.14–1.15), Eu/Eu^*_{MuQ} is always positive (1.01–2.02), and Y/Y^*_{MuQ} is weakly to strongly positive (1.13–2.02) (Fig. 7, Table 3). Y/Ho ratios are weakly to strongly super-chondritic (29.1–51.5) in all samples (Fig. 7).

3.2.5. Relative influences of geochemical reservoirs

Mixing line diagrams show that these bulk samples generally indicate some contribution from hydrothermal activity: Eu/Sm *versus* Sm/Yb plots show that Middle Marker horizon samples indicate only 0.5–2% hydrothermal contribution, those of the Hooggenoeg H5 chert show 2–6% contribution, samples from the Footbridge Chert 3.5–5%, and those of the Josefsdal Chert 0.5–5% (though most Josefsdal Chert samples fall between 2 and 5%) (Fig. 7C). Y/Ho *versus* $(Pr/Nd)_{MuQ}$ diagrams, though qualitative, and for comparative use only, suggest that the influence of seawater was greater in the Josefsdal Chert and Middle Marker horizon than in the Hooggennoeg H5 chert and the Footbridge Chert samples (Fig. 7D). La and Eu anomalies fall within the regions of values delimited by previous analyses of fossiliferous sedimentary cherts (e.g. Sugahara et al., 2010), although La anomalies in our samples are generally lower. In these other cherts, increased terrigenous contribution is signified by the closeness of points to the end-member reflecting the chemical characteristics of the MuQ composite.

3.3. In situ LA ICP-MS analyses

In Figs. 8–9, coloured curves and symbols refer to microbial horizons, whereas black curves and symbols refer to non-microbial horizons. These results are superimposed upon both bulk ICP-MS analyses and one another in the diagrams such that comparison between the fossiliferous and non-fossiliferous horizons may be easily made. All measured data are given in the Supplementary Tables.

3.3.1. Middle Marker horizon

In situ LA-ICP-MS analyses were conducted in three samples from the Middle Marker: two massive carbonaceous cherts (07SA22 and 07SA25) and one laminated, microbial mat-rich silicified volcaniclastic sandstone (07SA23) (Fig. 2A–B, S1). A transect of point analyses was taken through a thick microbial mat set within 07SA23, and point analyses were acquired at multiple ROIs within massive cherts, which lack clear stratigraphy.

In 07SA23 (Fig. 8A, 10A, Table 4), La/La^*_{MuQ} and Ce/Ce^*_{MuQ} show a slightly increased average within the mats. Eu anomalies are weakly negative and similar throughout the transect: below (0.77–1.17), within (0.83–1.37) and above (0.84–0.97) the mats. Finally, Y anomalies, weakly positive throughout, are again higher within the mat-rich layer. Y/Ho values are consistently chondritic to super-chondritic, ranging between 25.7 and 34.2 below the mats, 29.2–46.8 within, and 30.2–31.7 above, ergo, elevated within the mat-rich laminations (Fig. 10, S7, Table 4). For samples 07SA22 and 07SA25 (Fig. 8B, Table 4), La, Y, and Ce anomalies are positive (La/La^*_{MuQ} = 1.19 and 2.25, Y/Y^*_{MuQ} = 1.04 and 1.23 and Ce/Ce^*_{MuQ} = 1.07 and 1.40), whereas Eu anomalies are generally slightly negative to negligible (0.70 and 1.12). Y/Ho ratios are chondritic to super-chondritic, lower than in the silicified laminated chert, ranging from 25.3 to 34.5 (Fig. 10A, S8, Table 4).

Eu/Sm *versus* Sm/Yb mixing line plots show that most points are close to the seawater end-member. Sample 07SA23, a laminated sandstone–siltstone with well-developed microbial fabrics, indicates up to 1–2% hydrothermal contribution (Fig. 9A, coloured triangles). Massive carbonaceous chert, by contrast, indicates negligible hydrothermal contribution (Fig. 9A, black triangles). Terrigenous contribution is high in all samples: 30–95% of the pure MuQ signature in laminated chert (Fig. 9B, coloured triangles) and 70–100% in massive carbonaceous chert (Fig. 9B, black triangles).

3.3.2. Hooggenoeg chert H5c

Two further samples of Hooggenoeg Chert H5c were studied by *in situ* LA ICP-MS (Fig. 8C-D, Table 4): 03SA15, which includes thick (~1 cm) sequences of silicified microbial mats, and 03SA04, silicified, shallow-water, carbon-rich sediments. Transects were taken throughout the mat sequences, whereas for 03SA04, analyses were performed at several ROIs throughout the sample (Fig. 2C-D, S2).

For 03SA15 (Fig. 8C, 10B, Table 4), La/La^*_{MuQ} and Ce/Ce^*_{MuQ} are positive and broadly consistent throughout the transects, although La anomalies show a slight increase in the mat-rich layer. Eu/Eu^*_{MuQ} is weakly negative and broadly consistent throughout. Finally, Y/Y^*_{MuQ} markedly increases in the mat-rich layer. Y/Ho ratios are slightly elevated in the mat-bearing layer (Fig. 10B, S8; Table 4). In 03SA04 (Fig. 8D), La/La^*_{MuQ} = 1.43–2.98 (with three anomalous values of 16.01, 16.57 and 55.83), Ce/Ce^*_{MuQ} is 1.03–3.48 (with an anomalous value of 5.35), Eu/Eu^*_{MuQ} anomalies are variable and Y/Y^*_{MuQ} anomalies are weakly positive. Y/Ho ranges from 25.9 to 40.8 with all but one measurement yielding super-chondritic values (Fig. S7). In 03SA15, negligible hydrothermal contribution is suggested (Fig. 9C, coloured squares) but 78–100% of the pure MuQ signature denotes a significant terrigenous component (Fig. 9D, coloured squares), whereas for 03SA04, there is up to 2% contribution from hydrothermal fluids (Fig. 9C, black squares) and a terrigenous component of 50–90% of the pure MuQ signature (Fig. 9D, black squares).

3.3.3. Footbridge chert

In situ LA ICP-MS was performed on two further samples of shallow-water sediments from the Footbridge Chert. 03SA09 is a laminated black and white chert with copious microbial mat laminations, two of which were selected and analysed by transects (Fig. 2E, S3). 03SA09′ is a massive chert sampled from directly below 03SA09; the chert is nonetheless carbon-bearing, characterised by massive fabrics of clotted

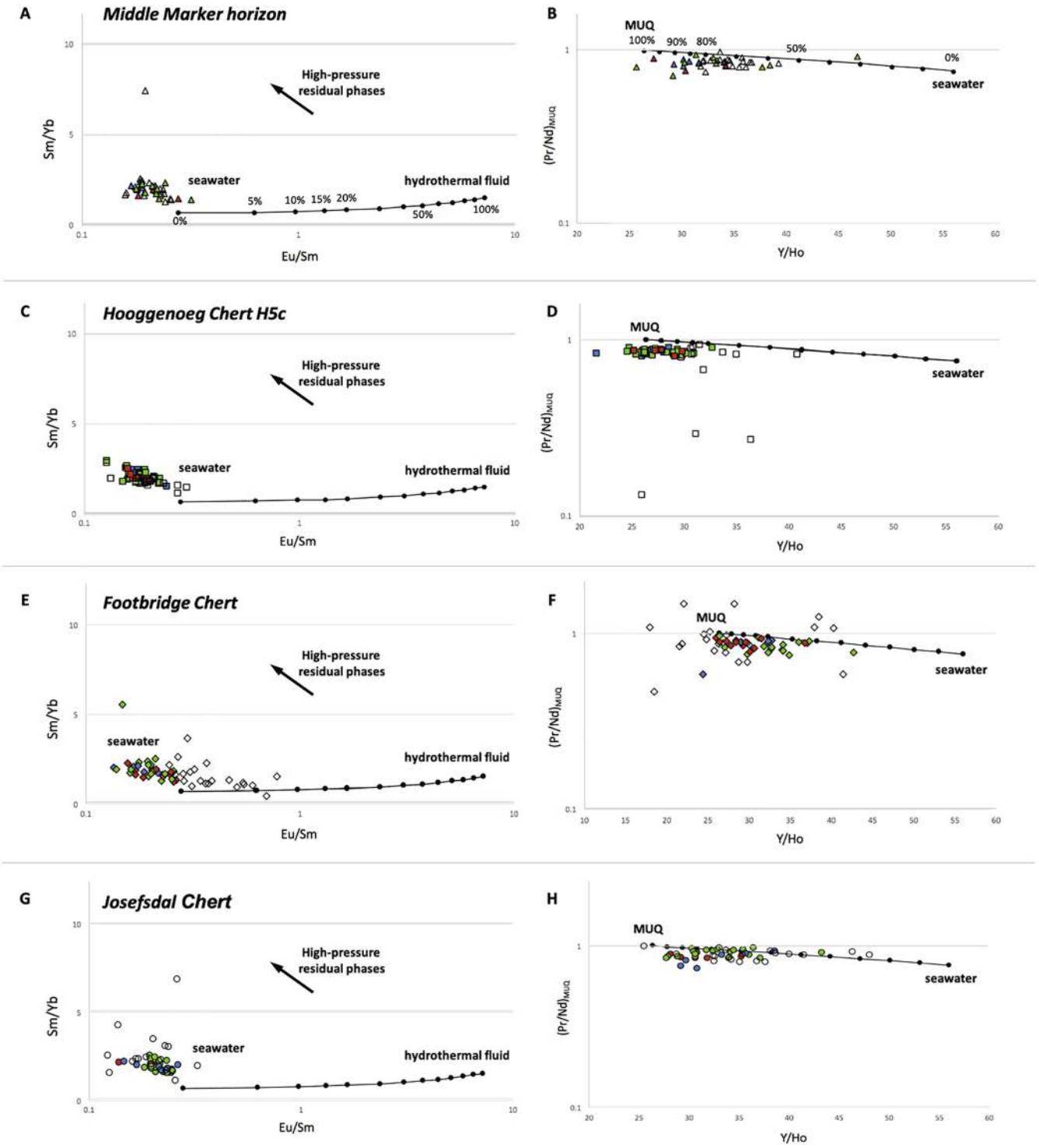

Fig. 9. *In situ* LA ICP-MS data plotted against mixing lines of hydrothermal fluid to seawater and seawater to MuQ-type terrigenous input, identical to those shown for bulk samples in Fig. 7. **A-B**) Middle Marker horizon; **C-D**) Hooggenoeg Chert H5c; **E-F**) Footbridge Chert; **G-H**) Josefsdal Chert. **A, C, E, G**) Eu/Sm *versus* Sm/Yb diagrams quantifying hydrothermal input. Points lying far above this mixing line (as with points of Sm/Yb > 5 in A and G) have incorporated high-pressure residual metamorphic phases, which overprint the original geochemical signatures. Coloured symbols represent series of analyses taken in microbial transects, unfilled symbols represent analyses taken in non-microbial horizons. Most microbial horizons record minor hydrothermal influence (negligible to 2%), whereas non-microbial horizons show elevated hydrothermal influence (up to 8%), i.e., non-microbial horizons plot closer to the hydrothermal end-member on the Eu/Sm *versus* Sm/Yb mixing line. **B, D, F, H**) Y/Ho *versus* Pr/Sm_{MuQ} plotted on a qualitative, conservative mixing line between seawater and MuQ, an idealised terrigenous input. Samples lying on or below this mixing line reflect the combined influenced of marine, terrigenous and hydrothermal fluid inputs, and samples which do not reach 100% terrigenous influence, i.e., 100% of the pure MuQ signal, may be considered "relatively less influenced" by terrigenous inputs (Gourcerol et al., 2016). Most samples are clustered around 60–100% MuQ, providing compelling evidence for the deposition of fossiliferous cherts in palaeoenvironments strongly influenced by terrigenous inputs (continental weathering). Red symbols indicate analyses taken below, green symbols analyses within, and blue symbols analyses above microbial horizons. Unfilled symbols are analyses conducted in non-microbial horizons. Sample analysed are as follows: Middle Marker horizon, coloured symbols = 07SA23, unfilled symbols = 07SA22, 07SA25; Hooggenoeg Chert H5c, coloured symbols = 03SA15, unfilled symbols = 03SA04; Footbridge Chert, coloured symbols = 03SA09, unfilled symbols = 03SA09'; Josefsdal Chert, coloured symbols = 12SA18, 12SA36, unfilled symbols = 99SA07. (For interpretation of the references to colour in this figure legend, the reader is referred to the web version of this article.)

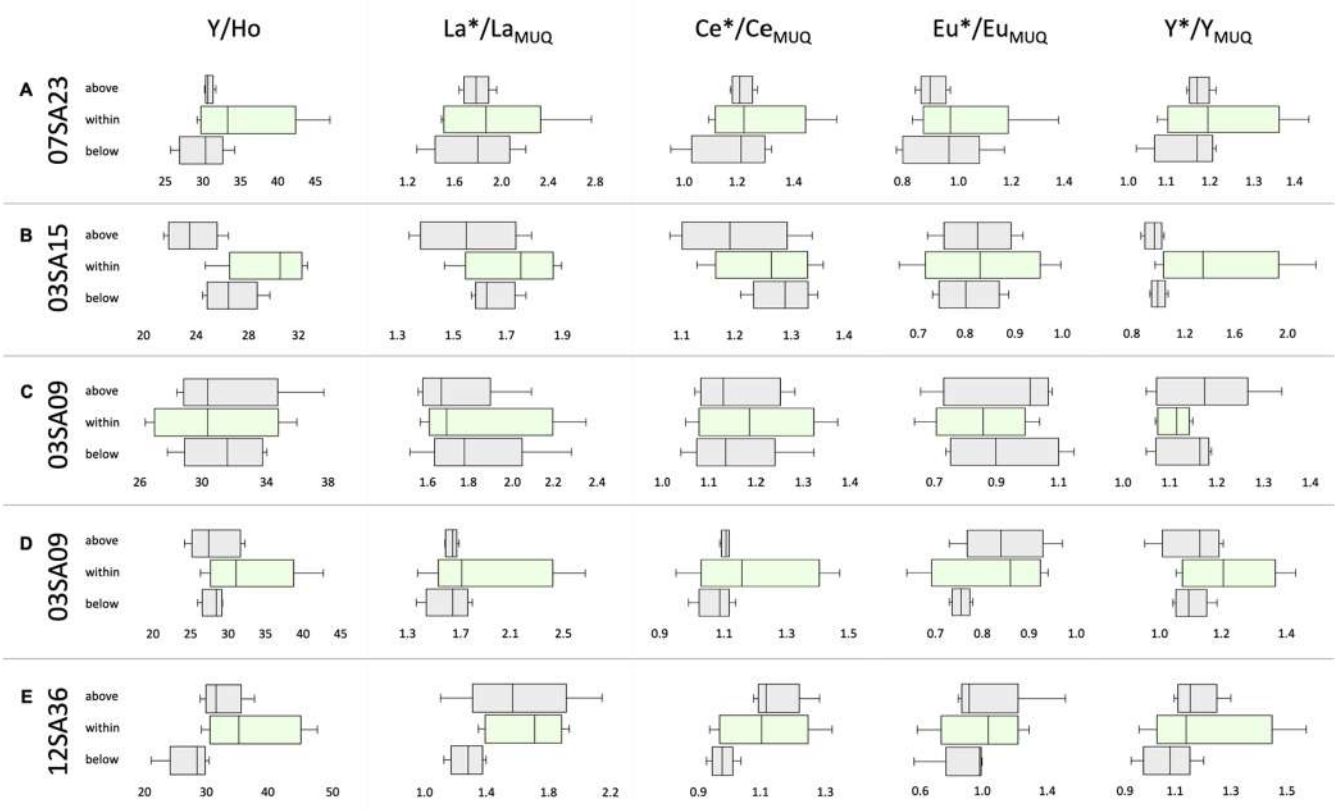

Fig. 10. Box plots showing representative *in situ* LA ICP-MS transect analyses of microbial horizons from the studied samples: **A)** Middle Marker horizon; **B**) Hooggenoeg chert H5c, **C-D)** Footbridge Chert (two horizons shown); **E**) Josefsdal Chert. For each sample, LA ICP-MS point analyses were conducted below, within and above the microbial horizons (see schematic in Fig. 1). For each of the transects, changes in Y/Ho ratio and La, Ce, Eu and Y anomalies (La/La*$_{MUQ}$, Ce/Ce*$_{MUQ}$, Eu/Eu*$_{MUQ}$ and Y/Y*$_{MUQ}$) were evaluated. Grey boxes represent analyses within chert above and below microbial layers, whereas green boxes represent analyses taken in chert within microbial layers. The vertical line within the box reports the median value, while the left and right edge of the box are the 25th and 75th percentile, respectivley. Y/Ho ratio, La and Y anomalies generally show statistically significant increases within microbial horizons, whereas Ce anomalies sometimes increase, and Eu anomalies show no significant changes. (For interpretation of the references to colour in this figure legend, the reader is referred to the web version of this article.)

and disseminated carbonaceous material (Fig. 2F), and analyses were taken from ROIs throughout this sample. MuQ-normalised REE + Y patterns for the mat-bearing sample 03SA09 are very flat, indicating considerable terrigenous influence (Fig. 8E-F), whereas those of massive chert 03SA09′ bear hallmarks of typical marine patterns (Fig. 8G).

For 03SA09 (Fig. 8E-F, 10C-D, Table 4), La/La*$_{MuQ}$ anomalies increase within one of the two studied mat-bearing horizons, but increase in chert above the second. Ce/Ce*$_{MUQ}$ also increases within one mat-bearing horizon. Eu/Eu*$_{MuQ}$ values are negative and consistent throughout the transects. Finally, Y/Y*$_{MuQ}$ anomalies also increase within one mat-bearing layer and Y/Ho ratios show a slight increase within the mat-bearing layers (Fig. 10C-D). Eu/Sm *versus* Sm/Yb diagrams estimate a negligible to 1% hydrothermal component (Fig. 9E), since almost all points plot to the left of the seawater end of the mixing curve. The estimated terrigenous component is between 45% and 100% of the pure MuQ signature (Fig. 9F). In 03SA09′ (Fig. 8G), remarkably different characteristics in REE + Y patterns emerge. La/La*$_{MuQ}$ ranges from negative to strongly positive (0.41–6.13), Ce/Ce*$_{MuQ}$ is negative to positive (0.55–2.67), Eu/Eu*$_{MuQ}$ is weakly to strongly positive (1.21–2.87), and Y/Y*$_{MuQ}$ is weakly positive (0.83–1.47). Y/Ho values range from 18.1 to 41.8 (Fig. S9). In contrast to the mat-bearing sample, the quantitative estimate of hydrothermal input suggests a contribution of up to 8% (Fig. 9E), but the terrigenous contribution is similar, between 50 and 100% of the pure MuQ signature (Fig. 9F).

3.3.4. *Josefsdal chert*

In situ LA ICP-MS was conducted on three further samples of Josefsdal Chert. 12SA18 and 12SA36 are two shallow-water sediments with well-developed microbial mat horizons, which were analysed, as for other mat-bearing samples, by transects bounded by chert layers (Fig. 1G, S4). The third sample, 99SA07, is a clotted carbonaceous chert comprising irregularly shaped carbonaceous clots within a silica matrix. Analyses were conducted at multiple ROIs throughout the sample (Fig. 1H, S4).

Within 12SA18 (Fig. 8H, 10E, Table 2), La/La*$_{MuQ}$, Ce/Ce*$_{MuQ}$ and Eu/Eu*$_{MuQ}$ increase upward through the transect. Y anomalies are constant through the transect. Y/Ho ratios show a slight increase within the mat-bearing layer. Within 12SA36 (Fig. 8I, Table 4), La anomalies are 1.12–1.39 below, 1.34–1.92 within and 1.10–2.13 above the mat. Ce anomalies are 0.92–1.03 below, 0.93–1.32 within and 1.07–1.28 above the mat. Eu anomalies are 0.56–0.99 below, 0.58–1.29 within and 0.84–1.52 above the mat. Y anomalies are 0.96–1.19 below, 0.95–1.57 within and 1.08–1.29 above the mat. Evidently, average La/La*$_{MuQ}$ and Y/Y*$_{MuQ}$ increase within mat-bearing layers (Fig. 10E). Y/Ho ratios also increases to superchondritic values within the mat-bearing layer (Table 4, Fig. 10E, S9). In 99SA07, Eu anomalies are considerably elevated (Eu/Eu*$_{MuQ}$ = 1.12–3.01; Fig. 8J) Eu/Sm *versus* Sm/Yb plots for the mat-rich sediments (12SA18 and 12SA36) suggest up to 1% hydrothermal contribution (Fig. 9G), and Y/Ho *versus* Pr/Nd$_{MuQ}$ diagrams indicate ~40–90% of the pure MuQ signature, i.e. some strong terrigenous contributions (Fig. 9H). 99SA07, by contrast, indicates up to 5% hydrothermal contribution (Fig. 9G) and terrigneous influences corresponding to 31–100% of the pure MuQ signature (Fig. 9H).

Table 3
Bulk ICP-MS bulk analyses.

A) Middle Marker	03SA01	07SA21	07SA22	07SA23
La/La*	0.7492	0.9337	0.9620	1.0949
Ce/Ce*	0.8081	1.0701	0.9057	0.9628
Y/Y*	0.5795	0.8460	0.9601	1.0735
Eu/Eu*	1.2978	1.4574	0.9758	1.3706
Y/Ho	17.747	22.006	24.821	29.287
Pr/Pr*	1.1104	0.9654	1.0073	1.0006
$(Pr/Yb)_{MUQ}$	0.1210	0.5321	0.4712	0.1747
Hydrothermal contribution	2%	2%	0.5%	2%
Detrital influence	100%	100%	100%	90%

B) Hooggenoeg Fm. H5c	01SA09	01SA56	03SA16	07SA28
La/La*	1.2244	0.8903	1.2210	1.1466
Ce/Ce*	1.0304	1.0304	0.9584	1.0033
Y/Y*	0.9754	0.9119	0.9909	0.9927
Eu/Eu*	1.6284	1.2886	2.1949	1.2325
Y/Ho	26.877	21.581	26.040	25.798
Pr/Pr*	0.9841	0.9841	1.0077	0.9713
$(Pr/Yb)_{MUQ}$	1.6608	2.8868	0.1657	0.2495
Hydrothermal contribution	4%	5%	6%	2%
Detrital influence	98%	100%	100%	100%

C) Footbridge Chert	*96SA02*	*12SA49*	*12SA50*
La/La*	0.9255	0.9390	1.0866
Ce/Ce*	0.9756	1.0022	1.0483
Y/Y*	1.0403	0.9757	0.9288
Eu/Eu*	1.1287	1.5265	1.9542
Y/Ho	25.785	23.942	23.628
Pr/Pr*	0.9979	0.9722	0.9713
$(Pr/Yb)_{MUQ}$	1.9598	3.5197	2.1157
Hydrothermal contribution	3.5%	5%	5%
Detrital influence	100%	100%	100%

D) Josefsdal Chert	14SA01	12SA16	12SA29	12SA06	12SA22	12SA10	12SA13	12SA32	12SA20	14SA04	12SA34	12SA01	12SA37
La/La*	0.8810	0.5321	2.9026	0.6778	0.9460	1.0116	0.9875	1.2185	1.8489	1.0466	1.1045	0.9322	1.0786
Ce/Ce*	0.7655	0.4676	1.5181	0.6307	0.7148	0.1417	0.9310	0.9598	1.1521	0.3528	0.8493	0.9303	0.7369
Y/Y*	1.3007	1.1259	1.4478	1.3288	1.1827	1.2303	1.1879	1.1907	1.2771	1.1653	1.4026	1.3688	1.1904
Eu/Eu*	2.0143	1.2753	1.5298	1.1746	1.7304	1.3436	1.4671	1.5981	1.0142	1.3418	2.0245	1.2306	1.5316
Y/Ho	32.024	32.953	38.5685	36.385	31.828	32.901	30.308	33.188	35.146	33.397	36.330	34.946	32.185
Pr/Pr*	1.1357	1.4591	0.7996	1.2568	1.1512	2.0442	1.0364	1.0206	0.9187	01.465	1.0807	1.0807	1.1505
$(Pr/Yb)_{MUQ}$	1.0732	0.7758	0.2439	1.2665	0.3238	2.4186	1.2312	0.5675	0.2092	2.0426	0.6817	1.1885	0.6547
Hydrothermal contribution	5%	2%	3%	0.5%	3.5%	2.5%	2.5%	3%	0.5%	2.5%	5%	2%	3%
Detrital influence	80%	78%	58%	67%	72%	78%	82%	77%	70%	76%	67%	71%	80%

3.3.5. 'Biome'-scale analyses: A summary of transect results from in situ LA ICP-MS

Transects were taken through chert domains within microbial mat horizons (Fig. 10; Table 4) to assess fine-scale changes in REE + Y composition during periods of microbial colonisation. These transect results indicate: i) the specific fluid chemistries of the environment encouraging the development of microbial ecosystems; and ii) whether alternation between microbial horizons and the surrounding cherts unveils cyclic palaeoenvironmental phenomena. As shown in Fig. 10, the results are similar across several millimetres of microstratigraphy within the four cherts studied:

- Y/Ho ratios increase from generally chondritic (~15–30) below the mat-bearing horizons to superchondritic values within (~25–50), before decreasing to chondritic values above the microbial mats;
- La and Y anomalies are generally more positive within mat-bearing horizons;
- Ce anomalies usually increase within the mat bearing horizons;
- Eu anomalies are generally consistently negative throughout microbial horizons, in contrast to the bulk analyses.

4 . Discussion

4.1. Characterisation of Palaeoarchaean regional habitats

The biosphere contains a diversity of biomes, defined as the community of organisms whose characteristics are common for the environments they dominate (i.e. a biospheric-geospheric entity), which in turn contain a number of ecosystems. In this section, we parameterise the palaeodepositional conditions in which the microbial communities preserved in the four studied cherts developed.

With the exception of the Footbridge Chert, MuQ-normalised patterns of bulk samples show HREE enrichment relative to LREE (Fig. 6), reflecting the differential dissolution of REE + Y into marine water as a function of ionic radii, surface and solution complexation stabilities, and oxidation onto oxyhydroxide particle surfaces (Bau, 1999; Allwood et al., 2010). The Footbridge Chert samples show negative slopes in MuQ-normalised REE + Y plots. Kamber et al. (2004) previously reported LREEs > HREEs in stromatolitic carbonate from the 2.8 Ga Mushandike Limestone of Zimbabwe, inferring the erosion of local sources (i.e., a strong continental input) and precipitation in a basin completely restricted from the open ocean. The MREE enrichment seen

Table 4
In situ LA ICP-MS biome analyses.

A) Middle Marker horizon	*07SA23 (microbial mat)*			*07SA22 and 07SA25(clotted/ clastic cherts)*
	below	*within*	*above*	
La/La*	1.27–2.20	1.48–2.76	1.63–1.95	1.19–2.25
Ce/Ce*	0.95–1.32	1.09–1.56	1.17–1.27	1.07–1.40
Y/Y*	1.02–1.21	1.07–1.43	1.14–1.21	1.04–1.23
Eu/Eu*	0.77–1.17	0.83–1.37	0.84–0.97	0.70–1.12
Y/Ho	25.7–34.2	29.2–46.8	30.2–31.7	25.3–34.5
$(Pr/Yb)_{MUQ}$	0.77			0.86
Hydrothermal contribution	Up to 2%			Negligible
Detrital influence	30–95%			70–100%

B) Hooggenoeg Fm. H5c	*03SA15 (microbial mat)*			*03SA04 (clastic chert)*
	below	*within*	*above*	
La/La*	1.57–1.77	1.47–1.90	1.34–1.79	1.43–2.98
Ce/Ce*	1.21–1.35	1.13–1.36	1.08–1.34	1.03–3.48
Y/Y*	0.94–1.08	0.98–2.22	0.87–1.05	1.01–1.28
Eu/Eu*	0.73–0.89	0.66–1.00	0.72–0.92	0.59–1.14
Y/Ho	24.5–29.7	24.7–32.6	21.5–26.5	25.9–40.8
$(Pr/Yb)_{MUQ}$	0.86			0.76
Hydrothermal contribution	Negligible			Up to 2%
Detrital influence	80–100%			50–90%

C) Footbridge Chert	*03SA09 (lower mat)*			*03SA09 (upper mat)*			*03SA09′ (clastic chert)*
	below	*within*	*above*	*below*	*within*	*above*	
La/La*	1.37–1.80	1.38–2.67	1.59–3.89	1.52–2.29	1.57–2.36	1.56–2.10	0.41–6.13
Ce/Ce*	0.99–1.14	1.08–1.47	1.09–1.75	1.04–1.28	1.05–1.37	1.07–1.28	0.55–2.67
Y/Y*	1.04–1.18	1.05–1.43	0.95–1.20	1.05–1.19	1.07–1.15	1.05–1.34	0.83–1.47
Eu/Eu*	0.73–0.78	0.64–1.02	0.73–0.97	0.73–1.14	0.63–1.03	0.65–1.07	1.21–2.87
Y/Ho	26.0–29.3	26.4–42.7	24.4–32.3	27.8–34.1	26.4–36.0	28.4–37.7	18.1–41.8
$(Pr/Yb)_{MUQ}$	0.80			0.80			0.80
Hydrothermal contribution	Negligible to 1%						Up to 8%
Detrital influence	45–100%						50–100%

D) Josefsdal Chert	*12SA18 (microbial mat)*			*12SA36 (microbial mat)*			*99SA07 (clotted chert)*
	below	*within*	*above*	*below*	*within*	*above*	
La/La*	1.45–1.83	1.35–1.88	1.51–2.28	1.12–1.39	1.34–1.92	1.10–2.13	1.03–3.28
Ce/Ce*	1.03–1.18	0.96–1.24	1.03–1.30	0.92–1.03	0.93–1.32	1.07–1.28	0.94–2.08
Y/Y*	1.03–1.25	1.03–1.36	1.09–1.35	0.92–1.19	0.95–1.57	1.08–1.29	0.74–1.32
Eu/Eu*	0.92–1.02	0.59–1.05	0.65–1.14	0.56–0.99	0.58–1.29	0.84–1.52	1.12–3.01
Y/Ho	27.9–34.1	27.8–43.2	29.2–38.5	21.2–30.4	29.2–46.7	29.0–37.6	19.1–42.2
$(Pr/Yb)_{MUQ}$	0.81			0.93			0.76
Hydrothermal contribution	Negligible to 1%						Up to 5%
Detrital influence	40–90%						31–100%

in 96SA02 along with increased V, Cr, Ni, Cu, As, Sn and W content (and therefore low Y/Ni and higher Cr/V; Fig. 11), suggests increased volcanogenic influence, likely from a dominantly komatiitic precursor (Hanor and Duchac, 1990; Nisbet and Fowler, 1999; Lowe and Byerly, 1999). We interpret these horizons of the Footbridge Chert as depositing in a comparable highly restricted basin setting, subjected to proximal subaerial volcanogenic input from komatiitic volcanism and with very limited, if any, exchange with the open ocean. Furthermore, in all other samples, despite their enrichment in HREE relative to LREE, the La/La^*_{MuQ}, Ce/Ce^*_{MuQ} and Y/Y^*_{MuQ} anomalies taken as diagnostic of hydrogenous sedimentation are often suppressed or negligible in bulk measurements. This is also consistent with deposition in semi-restricted conditions (Bau, 1999; Bolhar et al., 2015; Gourcerol et al., 2016), where inputs from continental weathering with high REE + Y concentrations dilute anomaly magnitudes (see also Kato and Nakamura, 2003). Notwithstanding, HREE enrichment (low $(Pr/Yb)_{MuQ}$), together with weakly positive La/La^*_{MuQ} and Y/Y^*_{MuQ}, indicate some marine influence. Overall, bulk MuQ-normalised REE + Y geochemistry indicates that all of these fossiliferous cherts show evidence for deposition in semi-restricted basins with variable marine influence resulting from periodic connection with the open ocean.

Eu/Eu^*_{MuQ} in bulk ICP-MS measurements is almost always positive (Figs. 6, 7B; Table 2). Customarily, positive Eu anomalies are ascribed to hydrothermal fluids, which are otherwise devoid of LREE or HREE enrichment and other anomalies (Danielson et al., 1992; Bau and Dulski, 1996; Allwood et al., 2010; Gourcerol et al., 2015). The often high REE + Y content of hydrothermal fluids relative to seawater (Klinkhammer et al., 1994; Wheat et al., 2002; Van Kranendonk et al., 2003; Tostevin et al., 2016) implies that hydrothermal inputs would, as with basin restriction, mathematically reduce hydrogenous anomalies, accounting for reduced La/La^*_{MuQ}, Ce/Ce^*_{MuQ} and Y/Y^*_{MuQ} in Archaean seawater relative to modern seawater, to which hydrothermal contributions are comparatively minor. The positive Eu/Eu^*_{MuQ} in bulk analyses (> 1.2 *cf.* Kerrich et al., 2013) therefore testifies to the regional significance of hydrothermal influence in Archaean habitable environments, which is likely a result of the advection of an Eu anomaly throughout the Archaean water column (Danielson, 1992; Sugahara et al., 2010; Allwood et al., 2010). Differences in Eu/Eu^*_{MuQ} between

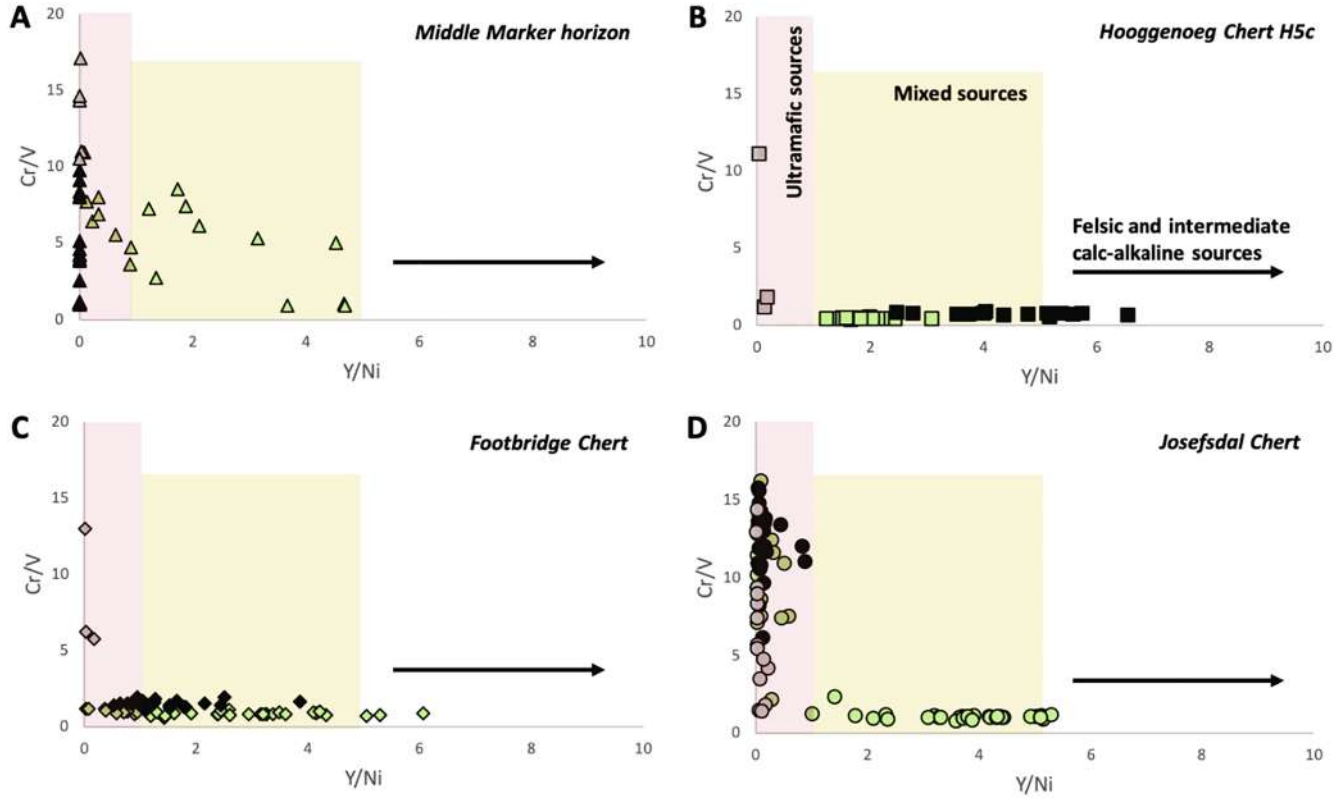

Fig. 11. Bulk ICP-MS and *in situ* LA ICP-MS results of Cr/V *versus* Y/Ni qualifying the relative importance of ultramafic (komatiitic-basaltic), felsic and calc-alkaline, and mixed source substrates (zones annotated in B). In all cases, bulk analyses (grey symbols) plot within the ultramafic field. With the exception of the Hooggenoeg Formation samples, *in situ* LA ICP-MS results from non-microbial chert horizons (black symbols) also suggest ultramafic precursors whereas LA ICP-MS analyses acquired within microbial horizons (green symbols) – including those for the Hooggenoeg chert – plot within the mixed sources field. This indicates that microbial colonisation correlates with periods of mafic-felsic mineralogical diversity associated with materials derived from continental weathering. (For interpretation of the references to colour in this figure legend, the reader is referred to the web version of this article.)

the Middle Marker sediments (up to 1.46) and those of the Hooggenoeg, Footbridge and Josefsdal cherts (up to 2.19, 1.95 and 2.02, respectively) may indicate either the relative influence of hydrothermal fluid or its temperature, i.e., a lesser quantity and/or lower temperature hydrothermal fluids may have influenced the Middle Marker horizon, and greater quantity and/or higher-temperature fluids the other studied units.

Chondritic Y/Ho values together with positive Eu/Eu^*_{MuQ} and low La/La^*_{MuQ} and Y/Y^*_{MuQ} in the Middle Marker horizon, Hooggenoeg Chert H5c and Footbridge Chert (Fig. 7, S7) denote that precipitation on the regional scale was strongly influenced by non-marine inputs; due to the positive Eu/Eu^*_{MuQ}, this is seemingly most parsimoniously explained as fluids of hydrothermal origin (*cf.* Bolhar et al., 2005). Nonetheless, the relative flatness of some patterns (i.e. high LREE concentrations) denotes appreciable terrigenous input (Hoyle et al., 1984; Elderfield et al., 1990; Bolhar and Van Kranendonk, 2007). As indicated above, even though the Josefsdal Chert shows superchondritic Y/Ho ratios, i.e., marine input, the consistently high concentrations of LREE are also testament to strong terrigenous input. Of the four studied cherts, we suggest that all were influenced by terrigenous contributes, but that the fossiliferous lithofacies of the Josefsdal Chert were relatively most influenced by interaction with the open ocean (Fig. 7C–D). This is sustained by the superchondritic Y/Ho ratios in Josefsdal Chert samples, together with stronger La, Eu and Y anomalies (Fig. 7A–B) that denote the influence of seawater with hydrothermal fluid signals advected throughout the water column. Previous trace and REE palaeoenvironmental reconstructions from Archaean cherts have found little evidence for such strong terrigenous influence before the Mesoarchaean (3.0–2.9 Ga), the most ancient examples of similar environmental setting being those from the Pongola Supergroup (Bolhar et al., 2015) and Mount Goldsworthy greenstone belt (Sugahara et al., 2010). Only Kato and Nakamura (2003) have convincingly suggested exposed granitoid-like bodies, though the extent of these bodies is uncertain. Our findings are thus inconsistent with the prevailing view of exposed Archaean landmasses as very minor volcanic islands (see references in Section 1.1.) and suggest that significant exposed continental landmasses featuring rivers with significant reach had already developed during the Palaeoarchaean. The initiation of continent building is proposed to have commenced during the Palaeoarchaean (e.g. Cawood et al., 2018), and the less fractionated REE + Y patterns reported herein support such early development of subaerial landmasses.

Overall, the bulk REE + Y patterns (ICP-MS results) for all studied units indicate a complex redox scenario: the regional environment within which widespread, shallow-water,Palaeoarchaean microbial mats flourished was characterised by hydrogenous sedimentary deposition with clear influence from non-marine sources, particularly terrigenous inputs and hydrothermal fluids (Figs. 6–7). In the Palaeoarchaean, terrigenous input would likely have mostly derived from the weathering of volcanogenic landmasses of dominantly mafic composition (Fig. 11).

In terms of geomorphology, the regional-scale environments of deposition of these four cherts were therefore semi-restricted water bodies with variable marine influence at the margins of emergent volcanic landmasses, a schematic of which is presented in Fig. 12. These *epicontinental basins* were subjected to inputs from seawater plus hydrothermal fluids, shown by their REE + Y patterns (Fig. 6) and their position on Eu/Sm *versus* Sm/Yb mixing lines (Fig. 7C), but also to strong influences from continental, volcanogenic, terrigenous material, evident both from high trace and REE contents (Figs. 5–6) and their

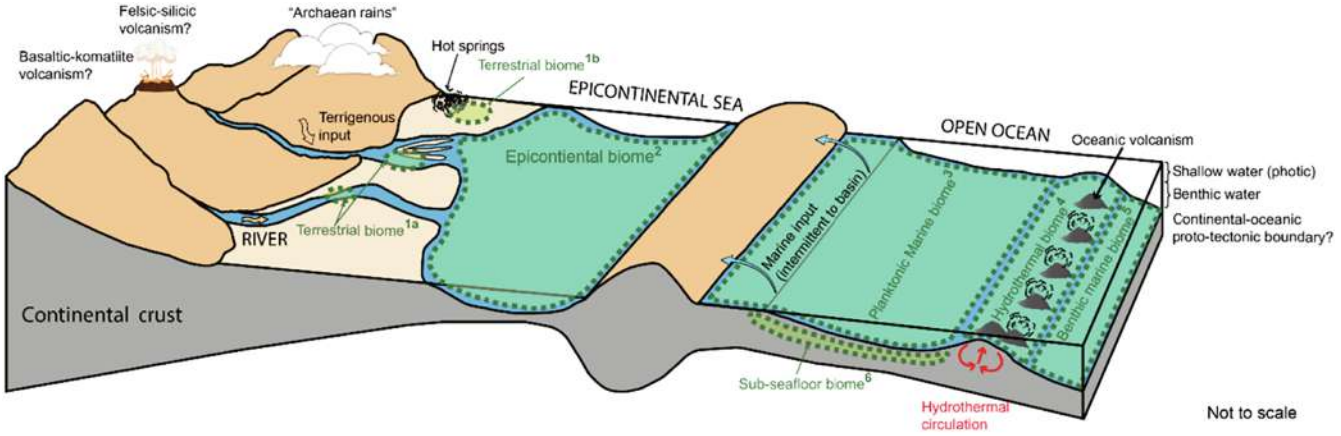

Fig. 12. A model for microbial biomes and their host environments throughout the Palaeoarchaean considering this study and a large volume of previous research. The epicontinental basin biome, outlined in this contribution, can be found at the centre of the diagram, perched atop the small landmass, with periodic restriction from the open ocean. The benthic marine biome colonises available seafloor in the presence of proximal and distal hydrothermal systems. Subjacent to the benthic marine biome is the sub-seafloor biome. Submarine and subaerial hydrothermal systems hosted thermophilic, chemosynthetic microbial life. Terrestrial fluvial and fluvio-deltaic siliciclastic systems were colonised by around 3.2 Ga, perhaps signalling a microbial evolutionary trajectory toward terrestrial-tolerant forms or reflecting the rise of ecological niches associated with modern-style continents. Finally, the planktonic marine biome is presumed though its unambiguous fossil record is less evident. The epicontinental basin biome occurs uniquely at the interface of the hydrosphere, atmosphere and lithosphere, and might therefore constitute an important driver or factor in biogeochemical cycles on the early Earth. The balance of these biomes was presumably driven by a combination of volcanic, marine, hydrothermal and riverine activity. Superscripts corresponding to each biome indicate example Archaean units: 1a) Fortescue Group (Bolhar and Van Kranendonk, 2007), Moodies Group (Homann et al., 2018); 1b) Dresser Formation (Djokic et al., 2017); 2) Mushandike Limestone (Kamber et al., 2004); Middle Marker horizon, Hooggenoeg Chert H5c, Footbridge Chert, Josefsdal Chert (this study); 3) Mount Goldsworthy-Mount Grant cherts (Suguhara et al., 2010; Sugitani, 2018), Kromberg Formation horizons (Walsh, 1992; Oehler et al., 2017); 4) Kangaroo Caves (Rasmussen, 2000); 5) Buck Reef Chert (Walsh, 1992; Tice and Lowe, 2006a,b; Greco et al., 2018), stratiform 'Apex chert' (Hickman-Lewis et al., 2016); 6) Sub-seafloor biome (Furnes et al., 2004, 2007).

position on $(Pr/Nd)_{MuQ}$ *versus* Y/Ho mixing lines (Fig. 7D). Previous field and petrographic evidence, showing copious sedimentary evidence for shallow-water deposition in shoreface and tidal shelf settings has indicated a coastal environmental setting for these cherts (Lanier and Lowe, 1982; Lowe and Byerly, 1999; Hofmann, 2011; Westall et al., 2015; Hickman-Lewis et al., 2018a), but the true significance of continental weathering inputs to these microbial biomes has been previously unrecognised. Nonetheless, the co-occurrence of terrigenous environments leading into semi-restricted epicontinental seas, eventually leading into the open oceans are consistent with geomorphological aspects of the hydrological cycle. Our findings of suppressed La, Eu and Y anomalies, together with the flat, LREE-enriched normalised REE + Y patterns characterising all studied microbial horizons is consistent only with REE + Y inheritance from continental outflow into basins having variably restricted communication with the open ocean. The chemistry of the source rocks may be estimated for these metasediments by separating the trace elements enriched in ultramafic, felsic and intermediate calc-alkaline, and mixed volcanic sources (Fig. 11). Plotting Y/Ni against Cr/V determined by bulk ICP-MS shows that all bulk samples plot clearly within the ultramafic field (Fig. 11), i.e., the predominant composition of the continental landmass in each case was mafic-komatiitic.

In restricted environments such as these, pH may be estimated from Ce/Ce^*_{MuQ}: when pH > 5, REE + Y patterns exhibit negative Ce/Ce^*_{MUQ}, whereas at pH < 5, a positive Ce/Ce^*_{MuQ} is generated (see Bau, 1999; Gourcerol et al., 2016). Although most samples show no 'true' Ce/Ce^*_{MuQ} (falling within Zone I of the Pr-Ce anomaly diagram of Bau and Dulski, 1996; Fig. S7), negative Ce/Ce^*_{MuQ} values in the Middle Marker horizon suggest that the unit deposited in an environment with pH ≥ 5. In the Josefsdal Chert, both alkaline and strongly acidic pH values are indicated, i.e. the ambient pH fluctuated, perhaps due to the presence of fluid cycling through volcanic glass before re-acting with overlying acidic seawater (Hofmann and Harris, 2007; Shibuya et al., 2010). Ce anomalies are insignificant in both the Hooggenoeg Chert H5c and the Footbridge Chert, suggesting either that the pH was around 5, which is consistent with some estimates of Archaean ocean pH (e.g. Pinti, 2005) or that the pH is indeterminable from the studied samples.

4.2. Characterisation of biomes preserved in Barberton cherts

Through a comparison of i) bulk ICP-MS analyses, quantifying the 'regional' or 'local'-scale redox landscape (Figs. 4–7, 11), and ii) *in situ* LA ICP-MS analyses quantifying the fluid chemistry of individual microbial horizons (Figs. 8–11), one can distinguish differences between the geochemistry of the microbial palaeoenvironment (the biome, this section) and its wider redox landscape (the habitat; Section 4.1.). In this section, we discuss exclusively the characteristics of Palaeoarchaean microbial biomes determined using transect LA ICP-MS analyses through mat-bearing horizons (*cf.* schematic in Fig. 1).

In all studied samples, REE + Y patterns in microbial horizons are notably flatter than the bulk signal (Fig. 8). Following the rationale above, this suggests that Palaeoarchaean photosynthetic biomass flourished where significant inputs from exposed continental landmasses influenced the habitat. Such inputs have high concentrations of LREE relative to hydrogenous deposition (Hoyle et al., 1984; Elderfield et al., 1990; Kato and Nakamura, 2003; Bolhar and Van Kranendonk, 2007). Both the REE + Y patterns of LA ICP-MS data and plots of these data onto Eu/Sm *versus* Sm/Yb and Y/Ho *versus* Pr/Nd_{MuQ} mixing lines suggest that all biomes were influenced by seawater, terrigenous inputs and, to a lesser extent, hydrothermal fluids (Figs. 8 and 9). The higher absolute concentration of REE + Y, especially high LREE and the almost complete suppression of anomalies in the patterns (Fig. 8) is consistent with dominantly riverine-derived aqueous chemistries. Y/Ho *versus* Pr/Nd_{MUQ} diagrams show significant terrigenous contributions in the four studied units (Fig. 9) compared to, for example, Precambrian banded iron formations (Gourcerol et al., 2016) or microbial carbonates (Van Kranendonk et al., 2003; Allwood et al., 2010). Mostly sub-chondritic and supra-chondritic Y/Ho ratios suggest limited seawater influence. Eu/Sm *versus* Sm/Yb mixing line calculations quantitatively estimate that, while microbial biomes themselves show low (negligible to 2%) hydrothermal contribution, the local environment (habitat;

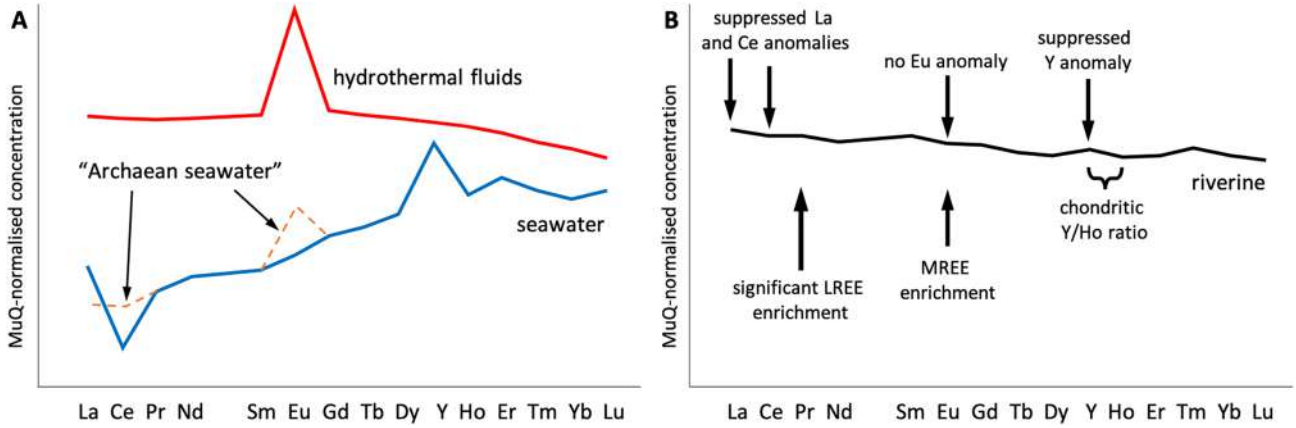

Fig. 13. Summary of the REE + Y characteristics of common aqueous reservoirs. **A**) MuQ-normalised REE + Y patterns of modern seawater (blue line), the changes to seawater-like signals common in Archaean marine sediments due to the influences of anoxic palaeodepositional conditions and enhanced hydrothermal activity (orange lines superposed onto blue line) and hydrothermal fluids (red line). **B**) Typical MuQ-normalised REE + Y trend for riverine sediments showing the characteristics exhibited by riverine-type patterns described herein, specifically the flat trend at enriched REE + Y concentrations, the suppression of La, Ce, Eu and Y anomalies, chondritic to sub-chondritic Y/Ho ratios and enrichments in LREE (significant) and MREE (moderate). (For interpretation of the references to colour in this figure legend, the reader is referred to the web version of this article.)

Section 4.1.) was comparably more influenced (up to 8%). Therefore, widespread, presumably photosynthetic, microbial mats flourished during periods of decreased hydrothermal input, correlating with decreased volcanism and increased local erosion and input of terrigenous material. Indeed, all studied horizons are essentially volcanogenic (Lanier and Lowe, 1982; Walsh, 1992; Lowe, 1999; Lowe and Byerly et al., 1999; Westall et al., 2015).

Whereas non-microbial horizons and all bulk samples plot within the ultramafic region of the Y/Ni *versus* Cr/V plot, microbial horizons plot dominantly within the mixed sources region, denoting that the influx of continental weathered substrate seems to have been more mineralogically diverse during periods of microbial colonisation (Fig. 11). Such correlation between the flourishing of microbial life and the evolved or fractionated nature of the substrate underlines the importance of small emerged landmasses – of greater lithological and mineralogical diversity than oceanic crust due to subaerial weathering – as loci of well-developed microbial communities. We propose that this is a consequence of both the wide range of bio-functional elements provided by mixed igneous source rocks, and the disequilibrium conditions present in basins characterised by the confluence of mixed fluid inputs. An ever-evolving interplay between sedimentation, ocean chemistry and microbiology thus led to widespread epibenthic Palaeoarchaean biomes occupying a delicate, complex biogeochemical niche driven by fluid inputs (Fig. 9), substrates (Fig. 11) and physical constraints resulting from volcanogenic sedimentation (Fig. 12). Such complex geochemical conditions would certainly have resulted in a diversity of metabolic pathways used by microbes in the biome. Within tens to hundreds of metres of lateral continuity in the ecosystem, it is likely that thermophilic organisms dependent upon hydrothermal heat and nutrients and non-thermophiles without such requirements, coexisted. The microbial mats studied herein appear to represent the latter group.

Although the LA ICP-MS patterns appear flat, they retain, particularly within microbial horizons, the superchondritic Y/Ho ratios and weak anomaly characteristics of seawater, which are marginally strengthened in layers of biomass relative to the surrounding non-microbial layers (compare green and grey boxes in Fig. 10). Although oxyhydroxides, which are enriched within microbial layers, select Ho over Y, the chondritic/sub-chondritic Y/Ho ratios expected in microbial mats (Censi et al., 2013) are not observed in our mat transect analyses. Furthermore, we can discount a control of the REE + Y signal by sedimentary organic matter (Takahashi et al., 2005; Freslon et al., 2014), both since we analysed only chert (SiO_2) within fossiliferous horizons, and not the organic material itself, and since we do not observe the MREE and HREE enrichments associated with scavenging by organic matter. The small-scale anomaly and Y/Ho fluctuations observed through the transects (Fig. 10) are thus primary and indicate that periodic seawater recharge into the basin drove microbial colonisation of nutrient-rich, mineralogically diverse substrates during periods of fluid disequilibrium between hydrothermally influenced marine influx and terrigenous outflow. These fluctuations underscore the semi-restricted nature of the basins (Fig. 12).

The negative Eu/Eu^*_{MuQ} in transect analyses may partly result from inner sphere MREE binding onto carboxylate and phosphate sites in microbial cellular and extracellular material (Censi et al., 2013) of autochthonous and allochthonous origins, for example relict biogenic detritus, rip-up and roll-up mat fragments, EPS and other macromolecular carbon. This is, however, inconsistent with the lack of evidence for any other interaction between organic materials and REE in these samples. Gao and Wedepohl (1995) suggested that the negative Eu/Eu^*_{MuQ} in some Archaean rocks is explained by the denudation of granitic-granitoid material in the source region. Kato and Nakamura (2003) also linked the erosion of differentiated and evolved plutonic/volcanic rocks, specifically granitoids, to negative Eu anomalies in metasediments from the Marble Bar greenstone belt. If such granite-granitoid chemistries interacted with the terrestrial hydrosphere during periods of alkaline aqueous chemistry, they could conceivable contribute to the negative Eu/Eu^*_{MuQ} in REE + Y signals in the resulting chemical precipitate. The question of negative Eu^*/Eu_{MuQ} nonetheless remains open to discussion.

To summarise this section, our LA ICP-MS transect analyses demonstrate that exposed landmasses (continents) in the Palaeoarchaean provided oases around or upon which well-developed microbial biomes flourished (Fig. 12). These biomes were characterised by a complex interplay of marine and riverine chemistries resulting in MuQ-normalised REE + Y patterns with the characteristics shown in Fig. 13. Since REE + Y patterns rapidly fractionate in estuarine settings (e.g., Elderfield et al., 1990; Bau, 1999), the endurance of the riverine pattern observed in our results necessitates a significant degree of basin restriction and/or well-developed river systems. Anastomosing river systems with long reaches are consistent with greenstone belt architecture (Krapez and Barley, 1987; Thurston, 2015) and with the maintenance of riverine-type REE + Y chemistry in the sedimentary record. Ecosystems within the epicontinental basin biome reconstructed herein may have repeatedly proliferated as a function of diverse mineralogies provided by mafic-felsic (continental) weathering inputs

(Fig. 11) together with periodic basin recharge by seawater (elevated Y/Ho and positive La/La^*_{MuQ} and Y/Y^*_{MuQ}).

The fact that this river-influenced epicontinental signature is recurrently identified in the four studied horizons, collectively spanning 150 Ma, which corresponds to much of the Palaeoarchaean fossil record of South Africa, implies that emergent landmasses were relatively common at this time. Evidence for the subaerial exposure of landmasses (Kato and Nakamura, 2003; Westall et al., 2011; Sugahara et al., 2010; Djokic et al., 2017; Homann et al., 2018) and the development of major crustal bodies of importance to the process of continent-building (Hickman, 2012; Kamber, 2015; Van Kranendonk et al., 2015; Dhuime et al., 2015; Cawood et al., 2018) are increasingly reported from Early Archaean sequences. Our findings substantiate that partially restricted epicontinental basins – likely resulting from the changing nature of global crust, and the rigidity of the resulting continental materials – provided the ideal regional geomorphological and geochemical theatres to sustain widespread biomes of early life. The epicontinental basin biome may have been as important to global biogeochemical cycling as oceanic biomes, and may have served as an intermediate stage between the earliest life at oceanic hydrothermal regions (Nisbet and Fowler, 1996, 1999) and the first conquest of land by approximately 3.2 Ga (Homann et al., 2018). Denoting the fine-scale characteristics of the hitherto unrecognised Palaeoarchaean epicontinental basin biome was possible only through coupling bulk and *in situ* trace and REE systematics.

4.3. Biome reconstruction in the Archaean

The REE + Y patterns reported within these microbial horizons are unique for the Palaeoarchaean (Fig. 8). Although most previous REE + Y studies of carbonaceous cherts have suggested overwhelmingly marine palaeodepositional environments for fossil-bearing cherts (e.g. Kamber and Webb, 2001; Van Kranendonk et al., 2003; Hofmann and Bolhar, 2007; Hofmann and Harris, 2008; Allwood et al., 2010), we suggest that this might be an issue of analytical scale, evident in that the bulk ICP-MS analyses herein produced similar results, distinct from *in situ* laser ablation analyses. Bulk analyses are not, however, applicable at microbially relevant resolutions.

Terrigenous, epicontinental sea-type biomes as described herein had, prior to this study, been found only in units up to 3.0 Ga (Grassineau et al., 2002; Kamber et al., 2004; Bolhar and Van Kranendonk, 2007; Sugahara et al., 2010; Stüeken et al., 2017). Terrestrial palaeoenvironments in the Moodies Group (Homann et al., 2018) and the Dresser Formation (Djokic et al., 2017) suggest that exposed landmasses may also have permitted an Archaean biome adjacent to the presumably more widespread epicontinental marine biome described herein, but only in the case of the Moodies Group has the regional significance of the biome been demonstrated. In the Palaeoarchaean, the limited recognition of terrigenous signals likely results from the masking of diagnostic parameters (such as Y/Ho ratios and the suppression of anomalies) by an overwhelmingly major marine hydrogenous signature in whole rock analyses.

Nisbet (1995, 2000), Nisbet and Fowler (1999) and Nisbet and Sleep (2001) presented the first palaeoecological hypotheses for the diverse biomes of Archaean life. As justly noted therein, at the time, much of our understanding of the distribution of life on the early Earth was *predicted* or *surmised* (Nisbet, 2000), but an increasing awareness of the range of biosignatures dating from the earliest geological record means that this is no longer true. The distribution of early life was raised again a decade later by Brasier et al. (2011), who noted that a lack of appreciation of the diversity of early life may also result from a reductionist prejudice to focus only on a restricted range of environments.

Environmental evolution through the early stages of Earth history follows an anaerobic to aerobic evolutionary trajectory (Knoll et al., 2016). This trajectory is presumably linked to the progressive opening of ecological niches as the mineralogy of the Earth diversified. The Palaeoarchaean marine realm was doubtless characterised by a rich diversity of microbial life, both in shallow-water coastal environments and possibly within the water column (Nisbet, 2000; Nisbet and Sleep, 2001; Hickman-Lewis et al., 2018b; Sugitani, 2018). Chemosynthetic biomes in the deposits around hydrothermal vent systems and in the subseafloor are a further ecosystem which has yet to be fully appraised in the Archaean (Rasmussen, 2000; Furnes et al., 2004, 2007; Westall et al., 2015; McMahon and Ivarsson, 2019). Emergent and terrestrial niches inhabited by radiotolerant, halotolerant microbial life were seemingly a more minor biome, occurring sporadically throughout the ancient rock record (Westall et al., 2011; Djokic et al., 2017; Homann et al., 2018), although this could also be a function of palaeoenvironmental preservation potential. We here add a well-defined epicontinental basin biome to this suite (Fig. 12), which is habitable by virtue of the complex interactions of hydrogenous and terrigenous inputs within. The geochemical signatures of the epicontinental basin biome that elucidate its semi-restricted nature, summarised in Fig. 13, should be eminently discernible elsewhere in the geological record when analysed at similarly high microstratigraphic resolutions as herein.

Historical geobiology research is at a point of expansion: multiple scales of geological and geochemical assessment may unveil, as demonstrated through our analytical approach, similarities between fossiliferous units in deep time. This may allow the construction of a biogeographical model of the Archaean Eon which should yield biome-level evolutionary trajectories co-evolving with the geosphere. Such large-scale appraisals relevant to the co-evolution of Earth and Life, rather than traditional approaches of estimating the Archaean biogeochemical landscape on a microfossil-by-microfossil basis, provide a multi-resolution correlative palaeoecological lens through which biogeochemistry on the Archaean Earth may be reconstructed.

5. Conclusions

This contribution permits two conclusions advancing our current understanding of the biogeochemical landscape of the early Earth:

I) At high analytical resolutions, differences between the geochemical environment of early life (the biome) and that of the wider region (the habitat) are evident. Studies reporting exclusively shallow water marine depositional conditions for Archaean microbial mat-bearing cherts may have mistakenly made this conclusion as a result of conducting only bulk analyses in which fine-scale, fluctuating REE + Y signals are overwhelmed by signals reflecting the regional depositional environment. Herein, studying four microbial horizons spanning around 150 Ma, we have shown that complex fluid chemistries – driven by continental weathering – correlate with well-developed microbial mat ecosystems. This is consistent with modern biological oceanography: 50–75% of primary productivity occurs in disequilibrium interfaces close to riverine outputs into marine-dominated water bodies (Jeandel and Oelkers, 2015). Future geobiological studies must focus on multi-scalar geochemistry in order to identify the defining characteristics of the palaeo-biome.

II) Epicontinental basins fuelled by riverine waters from continental weathering (perhaps fluxes of rainfall; *cf*. Arndt and Nisbet, 2012) were regionally important biomes of the Palaeoarchaean. These biomes, existing at the hydrosphere-geosphere-atmosphere interface, were an anoxygenic "*Matworld*" (*cf*. Lenton and Daines, 2016) and were likely important in the regulation of biogeochemistry throughout deep time. Prior to globally distributed large continents, systems of Archaean basins (*cf*. Nijman et al., 2017) teeming with networks of anoxygenic microbial life extended across portions of the early Earth. Biome diversity would have increased during the Mesoarchaean-Neoarchaean, and again during the Great Oxygenation Event. Trajectories of emerging metabolic networks within such critical transitional periods may be observable through the reconstruction of biomes. This may be of particular interest for the

period between 3.2 and 2.7 Ga, during which much continental crust developed and available biological niches presumably diversified significantly.

Author contributions

KHL and BC conceived the research. BC and FW collected samples. KHL, DM and BC conducted the analyses. KHL, BG and DM treated the data. KHL wrote the paper with contributions from all authors. All authors contributed to discussion of the data.

Declaration of Competing Interest

The authors declare that they have no known competing financial interests or personal relationships that could have appeared to influence the work reported in this paper.

Acknowledgements

This work was funded by the INACMa project (Inorganic Nanoparticles in Archaean Carbonaceous Matter – A key to early life and palaeoenvironmental reconstructions; EU-FP7 Grant no. 618657) to BC and the French National Centre for Scientific Research (CNRS). KHL received support from the COST ORIGINS Action in the form of Grant no. TD1308-38914. We are grateful to Sylvain Janiec (ISTO-Orléans) for the production of thin sections. We further acknowledge the contributions of Martin Homann and an anonymous reviewer, whose constructive comments significantly improved the manuscript.

Appendix A. Supplementary data

Supplementary data to this article can be found online at https://doi.org/10.1016/j.precamres.2020.105689.

References

Alibo, D.S., Nozaki, Y., 1999. Rare earth elements in seawater: Particle association, shale-normalization, and Ce oxidation. Geochim. Cosmochim. Acta 63, 363–372.

Allwood, A.C., Grotzinger, J.P., Knoll, A.H., Burch, I.W., Anderson, M.S., Coleman, M.L., Kanik, I., 2009. Controls on development and diversity of Archean stromatolites. Proc. Natl. Acad. Sci. U.S.A. 106, 9548–9555.

Allwood, A.C., Kamber, B.S., Walter, M.R., Burch, I.W., Kanik, I., 2010. Trace element record depositional history of an Early Archean stromatolitic carbonate platform. Chem. Geol. 270, 148–163.

Arndt, N.T., Nisbet, E.G., 2012. Processes on the young earth and the habitats of early life. Annu. Rev. Earth Planet. Sci. 40, 521–549.

Bartley, J.K., 1996. Actualistic taphonomy of cyanobacteria: Implications for the precambrian fossil record. Palaios 11, 571–586.

Bau, M., 1999. Scavenging of dissolved yttrium and rare earths by precipitating iron oxyhydroxide: experimental evidence for Ce oxidation, Y-Ho fractionation, and lanthanide tetrad effect. Geochim. Cosmochim. Acta 63, 67–77.

Bau, M., Dulski, P., 1996. Distribution of yttrium and rare-earth elements in the Penge and Kuruman iron-formations, Transvaal Supergroup, South Africa. Precambr. Res. 79, 37–55.

Bolhar, R., Van Kranendonk, M.J., 2007. A non-marine depositional setting for the northern Fortescue Group, Pilbara Craton, inferred from trace element geochemistry of stromatolitic carbonates. Precambr. Res. 155, 229–250.

Bolhar, R., Kamber, B.S., Moorbath, S., Fedo, C.M., Whitehouse, M.J., 2004. Characterisation of early Archaean chemical sediments by trace element signatures. Earth Planet. Sci. Lett. 222, 43–60.

Bolhar, R., Van Kranendonk, M.J., Kamber, B.S., 2005. A trace element study of siderite-jasper banded iron formation in the 3.45 Ga Warrawoona Group, Pilbara Craton-Formation from hydrothermal fluids and shallow seawater. Precambr. Res. 137, 93–114.

Bolhar, R., Hofmann, A., Siahi, M., Feng, Y.-X., Delvigne, C., 2015. A trace element and Pb isotopic investigation into the provenance and deposition of stromatolitic carbonates, ironstones and associated shales of the ~3.0 Ga Pongola Supergroup, Kaapvaal Craton. Geochim. Cosmochim. Acta 158, 57–78.

Brasier, M.D., Wacey, D., McLoughlin, N., 2011. Taphonomy in temporally unique settings: An environmental traverse in search of the earliest life on Earth. In: Allison, P.A., Bottjer, D.J. (Eds.), Taphonomy: Process and Bias Through Time, Topics in Geobiology 32. Springer, pp. 487–518.

Cawood, P.A., Hawkesworth, C.J., Pisarevsky, S.A., Dhuime, B., Capitanio, F.A., Nebel, O., 2018. Geological archive of the onset of plate tectonics. Phil. Trans. R. Soc. London A 376, 20170405.

Censi, P., Cangemi, M., Brusca, L., Madonia, P., Saiano, F., Zuddas, P., 2013. The behavior of rare-earth elements, Zr and Hf during biologically-mediated deposition of silica-stromatolites and carbonate-rich microbial mats. Gondwana Res. 27, 209–215.

Danielson, A., Möller, P., Dulski, P., 1992. The europium anomalies in banded iron formations and the thermal history of the oceanic crust. Chem. Geol. 97, 89–100.

De Carlo, E.H., Green, W.J., 2002. Rare earth elements in the water column of Lake Vanda, McMurdo Dry Valleys, Antarctica. Geochim. Cosmochim. Acta 66, 1323–1333.

De Gregorio, B.T., Sharp, T.G., 2006. The structure and distribution of carbon in the 3.5 Ga Apex chert: Implications for the biogenicity of Earth's oldest putative microfossils. Am. Mineral. 91, 784–789.

Dhuime, D., Wuestefeld, A., Hawkesworth, C.J., 2015. Emergence of modern continental crust about 3 billion years ago. Nat. Geosci. 8, 552–555.

Djokic, T., Van Kranendonk, M.J., Campbell, K.A., Walter, M.R., Ward, C.R., 2017. Earliest signs of life on land preserved in 3.5 Ga hot spring deposits. *Nature.* Communications 8, 15263.

Elderfield, H., Upstill-Goddard, R., Sholkovitz, E.R., 1990. The rare earth elements in rivers, estuaries, and coastal seas and their significance to the composition of ocean waters. Geochim. Cosmochim. Acta 54, 971–991.

Freslon, N., Bayon, G., Toucanne, S., Bermell, S., Bollinger, C., Chéron, S., Etoubleau, J., Germain, Y., Khripounoff, A., Ponzevera, E., Rouget, M.-L., 2014. Rare earth elements and neodymium isotopes in sedimentary organic matter. Geochim. Cosmochim. Acta 140, 177–198.

Furnes, H., Banerjee, N.R., Muehlenbachs, K., Staudigel, H., de Wit, M.R., 2004. Early life recorded in Archean pillow lavas. Science 304, 578–581.

Furnes, H., Banerjee, N.R., Staudigel, H., Muehlenbachs, K., McLoughlin, N., de Wit, M., Van Kranendonk, M., 2007. Comparing petrographic signatures of bioalteration in recent to Mesoarchean pillow lavas: tracing subsurface life in oceanic igneous rocks. Precambr. Res. 158, 156–176.

Gao, S., Wedepohl, K.H., 1995. The negative Eu anomaly in Archean sedimentary rocks: Implications for decomposition, age and importance of their granitic sources. Earth Planet. Sci. Lett. 133, 81–94.

Gourcerol, B., Thurston, P.C., Kontak, J.D., Côté-Mantha, O., 2015. Interpretations and implications of LA ICP-MS analysis of chert for the origin of geochemical signatures in banded iron formations (BIFs) from the Meadowbank Gold Deposit, Western Churchill Deposit, Nunavut. Chem. Geol. 410, 89–107.

Gourcerol, B., Thurston, P.C., Kontak, D.J., Côté-Mantha, O., Biczok, J., 2016. Depositional setting of Algoma-type banded iron formation. Precambr. Res. 281, 47–79.

Grassineau, N.V., Nisbet, E.G., Fowler, C.M.R., Bickle, M.J., Lowry, D., Chapman, H.J., Mattey, D.P., Abell, P., Yong, J., Martin, A., 2002. Stable isotopes in the Archaean Belingwe belt, Zimbabwe: evidence for a diverse microbial mat ecology. Geol. Soc. London Special Publ. 199, 309–328.

Greco, F., Cavalazzi, B., Hofmann, A., Hickman-Lewis, K., 2018. 3.4 Ga biostructures from the Barberton greenstone belt of South Africa: New insights into microbial life. Bollettino della Società Paleontologica Italiana 57, 59–74.

Hanor, J.S., Duchac, K.C., 1990. Isovolumetric silicification of early Archean komatiites; geochemical mass balances and constraints on origin. J. Geol. 98, 863–877. Hickman, A.H., 2012. Review of the Pilbara Craton and Fortescue Basin: Crustal evolution providing environments for early life. Isl. Arc 21, 1–31.

Hickman-Lewis, K., Garwood, R.J., Brasier, M.D., Goral, T., Jiang, H., McLoughlin, N., Wacey, D., 2016. Carbonaceous microstructures of the 3.46 Ga stratiform 'Apex chert', Chinaman Creek locality, Pilbara Western Australia. Precambr. Res. 278, 161–178.

Hickman-Lewis, K., Garwood, R.J., Withers, P.J., Wacey, D., 2017. X-ray micro-tomography as a tool for investigating the petrological context of Precambrian cellular remains. Geol. Soc. London Special Publ 448, 33–56.

Hickman-Lewis, K., Westall, F., Cavalazzi, B., 2018b. Trace of Early Life in the Barberton Greenstone Belt. In: Van Kranendonk, M.J., Bennett, V.C., Hofmann, J.E. (Eds.), Earth's Oldest Rocks, Second Edition, pp. 1029–1058.

Hickman-Lewis, K., Gautret, P., Arbaret, L., Sorieul, S., De Wit, R., Foucher, F., Cavalazzi, B., Westall, F., 2019. Mechanistic morphogenesis of organo-sedimentary structures growing under geochemically stressed conditions: Keystone to the interpretation of some Archaean stromatolites? Geosciences 9, 359.

Hickman-Lewis, K., Cavalazzi, B., Foucher, F., Westall, F., 2018a. Most ancient evidence for life in the Barberton greenstone belt: Microbial mats and biofabrics of the ~3.47 Ga Middle Marker horizon. Precambr. Res. 312, 45–67.

Hickman-Lewis, K., Cavalazzi, B., Sorieul, S., Gautret, P., Foucher, F., Whitehouse, M.J., Jeon, H., Cockell, C.S., Georgelin, T., Westall, F., 2020. Metallomics in deep time and the influence of ocean chemistry on the metabolic landscapes of Earth's earliest ecosystems. Sci. Rep.

Hofmann, A., 2011. Archaean hydrothermal systems in the Barberton greenstone belt and their significance as a habitat for early life. In: Golding, S.D., Glikson, M. (Eds.), Earliest Life on Earth: Habitats, Environments and Methods of Detection. Springer, Netherlands, pp. 51–78.

Hofmann, A., Bolhar, R., 2007. The origin of carbonaceous cherts in the Barberton greenstone belt and their significance for the study of early life in mid-Archaean rocks. Astrobiology 7, 355–388.

Hofmann, A., Wilson, A.H., 2007. Silicified basalts, bedded cherts and other sea floor alteration phenomena of the 3.4 Ga Nondweni greenstone belt, South Africa. In: Van Kranendonk, M.J., Smithies, R.H., Bennett, V.C. (Eds.), Earth's Oldest Rocks, Developments in Precambrian Geology 15, 571–605.

Hofmann, A., Harris, C., 2008. Stratiform alteration zones in the Barberton greenstone belt: A window into subseafloor processes 3.5 to 3.3 Ga ago. Chem. Geol. 257, 224–242.

Hofmann, A., Bolhar, R., Orberger, B., Foucher, F., 2013. Cherts of the Barberton

greenstone belt, South Africa: Petrology and trace-element geochemistry of 3.5 to 3.3 Ga old silicified volcaniclastic sediments. S. Afr. J. Geol. 116, 297–322.
Homann, M., Sansjofre, P., van Zuilen, M., Heubeck, C., Gong, J., Killingsworth, B., Foster, I.S., Airo, A., Van Kranendonk, M.J., Ader, M., Lalonde, S.V., 2018. Microbial life and biogeochemical cycling on land 3,220 million years ago. Nat. Geosci. 11, 665–671.
Hoyle, J., Elderfield, H., Gledhill, A., Greaves, M., 1984. The behavior of the rare earth element during mixing of river and sea waters. Geochim. Cosmochim. Acta 48, 143–149.
Jeandel, C., Oelkers, E.H., 2015. The influence of terrigenous particulate material dissolution on ocean chemistry and global element cycles. Chem. Geol. 395, 50–66.
Kamber, B.S., Webb, G.E., 2001. The geochemistry of late Archean microbial carbonate: Implications for ocean chemistry and continental erosion history. Geochim.
Cosmochim. Acta 65, 2509–2525.
Kamber, B.S., Bolhar, R., Webb, G.E., 2004. Geochemistry of late Archaean stromatolites from Zimbabwe: Evidence for microbial life in restricted epicontinental seas. Precambr. Res. 132, 379–399.
Kamber, B.S., Greig, A., Collerson, K.D., 2005. A new estimate for the composition of weathered young upper continental crust from alluvial sediments, Quennsland, Australia. Geochim. Cosmochim. Acta 69, 1041–1058.
Kamber, B.S., 2015. The evolving nature of terrestrial crust from the Hadean, through the Archaean, into the Proterozoic. Precambr. Res. 258, 48–82.
Kato, Y., Nakamura, K., 2003. Origin and global tectonic significance of Early Archean cherts from the Marble Bar greenstone belt, Pilbara Craton, Western Australia. Precambr. Res. 125, 191–243.
Kerrich, R., Said, N., Manikyamba, C., Wyman, D., 2013. Sampling oxygenated Archean hydrosphere: Implication from fractionations of Th/U and Ce/Ce* in hydrothermally altered volcanic sequences. Gondwana Res. 23, 506–525.
Klinkhammer, G.P., Elderfield, H., Edmond, J.M., Mitra, A., 1994. Geochemical implications of rare earth element patterns in hydrothermal fluids from mid-ocean ridges. Geochim. Cosmochim. Acta 58, 5105–5113.
Knoll, A.H., Barghoorn, E.S., 1977. Archean microfossils showing cell division from the Swaziland System of South Africa. Science 189, 396–398.
Knoll, A.H., Bergmann, K.D., Strauss, J.V., 2016. Life: The first two billion years. Phil. Trans. R. Soc. B: Biol. Sci. 371, 20150493.
Krapez, B., Barley, M.E., 1987. Archaean strike-slip faulting and related ensialic basins: Evidence from the Pilbara Block, Australia. Geol. Mag. 124, 555–567.
Lanier, W.P., Lowe, D.R., 1982. Sedimentology of the Middle Marker (3.4Ga), Onverwacht Group, Transvaal, South Africa. Precambr. Res. 18, 237–260.
Lawrence, M.G., Kamber, B.S., 2006. The behavior of the rare earth elements during estuarine mixing — Revisited. Mar. Chem. 100, 147–161.
Lawrence, M.G., Grieg, A., Collerson, K.D., Kamber, B.S., 2006. Rare earth element and yttrium variability in South East Queensland waterways. Aquat. Geochem. 12, 39–72.
Ledevin, M., Arndt, N., Simionovici, A., Jaillard, E., Ulrich, M., 2014. Silica precipitation triggered by clastic sedimentation in the Archean: New petrographic evidence from cherts of the Kromberg type section, South Africa. Precambr. Res. 255, 316–334.
Ledevin, M., Arndt, N., Chauvel, C., Jaillard, E., Simionovici, A., 2019. The sedimentary origin of black and white banded cherts of the Buck Reef, Barberton, South Africa. Geosciences 9, 424.
Lenton, T.M., Daines, S.J., 2016. Matworld – The biogeochemical effects of early life on land. New Phytol. https://doi.org/10.1111/nph.14338.
Lowe, D.R., 1999. Petrology and sedimentology of cherts and related silicified sedimentary rocks in the Swaziland Supergroup, vol. 329. Geological Society of America Special Publication, pp. 83–114.
Lowe, D.R., Byerly, G.R., 1999. Stratigraphy of the west-central part of the Barberton Greenstone Belt, South Africa. In: Lowe, D.R., Byerly, G.R. (Eds.), Geologic evolution of the Barberton Greenstone Belt, South Africa. Geological Society of America Special Paper 329, 1–36.
McMahon, S., Ivarsson, M., 2019. A New Frontier for Palaeobiology: Earth's Vast Deep Biosphere. BioEssays 41, 1900052.
Nijman, W., Kloppenburg, A., de Vries, S.T., 2017. Archaean basin margin geology and crustal evolution: An East Pilbara traverse. J. Geol. Soc. London 174, 1090–1112.
Nisbet, E.G., 1995. Archaean ecology: A review of evidence for the early development of bacterial biomes, and speculations on the development of a global-scale biosphere.
Geol. Soc. London Special Publ. 95, 27–55.
Nisbet, E.G., 2000. The realms of Archaean life. Nature 405, 625–626.
Nisbet, E.G., Fowler, C.M.R., 1999. Archaean metabolic evolution of microbial mats. Proc. R. Soc. London B: Biol. Sci. 266, 2375–2382.
Nisbet, E.G., Sleep, N.H., 2001. The habitat and nature of early life. Nature 409, 1083–1091.
Noffke, N., Christian, D., Wacey, D., Hazen, R.M., 2013. Microbially induced sedimentary structures recording an ancient ecosystem in the ca. 3.48 billion- year-old Dresser Formation, Pilbara, Western Australia. Astrobiology 13, 1103–1124.
Oehler, D.Z., Walsh, M.M., Sugitani, K., Liu, M.-C., House, C.H., 2017. Large and robust lenticular microorganisms on the young Earth. Precambr. Res. 296, 112–119. Orange, F., Westall, F., Disnar, J.-R., Prieur, D., Bienvenu, N., Le Romancer, M., Défarge, C., 2009. Experimental silicification of the extremophilic Archaea Pyrococcus abyssi and Methanocaldococcus jannaschii: applications in the search for evidence of life in early Earth and extraterrestrial rocks. Geobiology 7, 403–418.
Paris, I.A., Stanistreet, I.G., Hughes, M.J., 1985. Cherts of the Barberton greenstone belt interpreted as products of submarine exhalative activity. J. Geol. 93, 111–129.
Pinti, D., 2005. The origin and evolution of the oceans. In: In: Gargaud, M., Barbier, B., Martin, H., Reisse, J. (Eds.), Lectures in Astrobiology Volume I. Springer, pp. 83–112.
Rasmussen, B., 2000. Filamentous microfossils in a 3,235-million-year-old volcanogenic massive sulphide deposit. Nature 405, 676–679.
Robbins, L.J., Konhauser, K.O., Warchola, T.J., Homann, M., Thoby, M., Foster, I., Mloszewska, A.M., Alessi, D., Lalonde, S.V., 2019. A comparison of bulk versus laser ablation trace element analyses in banded iron formations: Insights into the mechanisms leading to compositional variability. Chem. Geol. 506, 197–224.
Schopf, J.W., Kudryavtsev, A.B., Osterhout, J.T., Williford, K.H., Kitajima, K., Valley, J.W., Sugitani, K., 2017. An anaerobic ~3400 Ma shallow-water microbial consortium: Presumptive evidence of Earth's Paleoarchean anoxic atmosphere. Precambr. Res. 299, 309–318.
Shibuya, T., Komiya, T., Nakamura, K., Takai, K., Maruyama, S., 2010. Highly alkaline, high-temperature hydrothermal fluids in the early Archean ocean. Precambr. Res. 182, 230–238.
Shields, G., Webb, G., 2004. Has the REE composition of seawater changed over geological time? Chem. Geol. 204, 103–107.
Stüeken, E.E., Buick, R., Anderson, R.E., Baross, J.A., Planavsky, N.J., Lyons, T.W., 2017. Environmental niches and metabolic diversity in Neoarchean lakes. Geobiology 15, 767–783.
Sugahara, H., Sugitani, K., Mimura, K., Yamashita, F., Yamamoto, K., 2010. A systematic rare-earth elements and yttrium study of Archean cherts at the Mount Goldsworthy greenstone belt in the Pilbara Craton: Implications for the origin of microfossil-bearing black cherts. Precambr. Res. 177, 73–87.
Sugitani, K., 2018. Early Archaean (pre-3.0 Ga) cellularly preserved microfossils and microfossil-like structures from the Pilbara craton, Western Australia – A review. In: Van Kranendonk, M.J., Bennett, V.C., Hofmann, J.E. (Eds.), Earth's Oldest Rocks, Second Edition, pp. 1007–1028.
Takahashi, Y., Châtellier, X., Hattori, K.H., Kato, K., Fortin, D., 2005. Adsorption of rare earth elements onto bacterial cell walls and its implication for REE sorption onto natural microbial mat. Chem. Geol. 219, 53–67.
Tankard, A.J., Jackson, M.P.A., Eriksson, K.A., Hobday, D.K., Hunter, D.R., Minter, W.E.L., 1982. Crustal evolution of southern Africa: 3.8 billion years of Earth history. Springer-Verlag, New York, pp. 523 p..
Thurston, P.C., 2015. Igneous Rock Associations 19. Greenstone belts and granite – Greenstone Terranes: Constraints on the nature of the archean world. Geosci. Can. 42, 437–484.
Thurston, P.C., Kamber, B.S., Whitehouse, M., 2012. Archean cherts in banded iron formation: Insight into Neoarchean ocean chemistry and depositional processes. Precambr. Res. 214–215, 227–257.
Tice, M.M., Bostick, B.C., Lowe, D.R., 2004. Thermal history of the 3.5–3.2 Ga Onverwacht and Fig Tree Groups, Barberton greenstone belt, South Africa, inferred by Raman microspectroscopy of carbonaceous material. Geology 32, 37–40.
Tice, M.M., Lowe, D.R., 2006a. Hydrogen-based carbon fixation in the earliest known photosynthetic organisms. Geology 34, 37–40.
Tice, M.M., Lowe, D.R., 2006b. The origin of carbonaceous matter in pre-3.0 Ga greenstone terrains: A review and new evidence from the 3.42 Ga Buck Reef Chert. Earth Sci. Rev. 76, 259–300.
Tostevin, R.E., Shields, G.A., Tarbuck, G.M., He, T., Clarkson, M.O., Wood, R.A., 2016. Effective use of Ce anomalies as a redox proxy in carbonate-dominated marine set-tings. Chem. Geol. 438, 146–162.
Van Kranendonk, M.J., Webb, G.E., Kamber, B.S., 2003. Geological and trace element evidence for a marine sedimentary environment of deposition and biogenicity of 3.45 Ga stromatolitic carbonates in the Pilbara Craton, and support for a reducing Archaean ocean. Geobiology 1, 91–108.
Van Kranendonk, M.J., Smithies, R.H., Griffin, W.L., Huston, D.L., Hickman, A.H., Champion, D.C., Anhaeusser, C.R., Pirajno, F., 2015. Making it thick: A volcanic plateau origin of Palaeoarchean continental lithosphere of the Pilbara and Kaapvaal cratons. Geol. Soc London Special Publ. 389, 83–111.
Wacey, D., 2009. Early life on earth, a practical guide. In: In: Landman, N.H., Harries, P.J. (Eds.), Topics in Geobiology, vol. 31 Springer, Heidelberg.
Walsh, M.M., 1992. Microfossils and possible microfossils from the Early Archean Onverwacht Group, Barberton Mountain Land, South Africa. Precambr. Res. 54, 271–293.
Walsh, M.M., Lowe, D.R., 1999. Modes of accumulation of carbonaceous matter in the early Archaean: A petrographic and geochemical study of the carbonaceous cherts of the Swaziland Supergroup. In: Lowe, D.R., Byerly, G.R. (Eds.), Geologic Evolution of the Barberton Greenstone Belt, South Africa. Geological Society of America Special Paper 329, Boulder, CO, pp. 115–132.
Westall, F., de Wit, M.J., Dann, J., van der Gaast, S., de Ronde, C.E.J., Gerneke, D., 2001. Early Archean fossil bacteria and biofilms in hydrothermally-influenced sediments from the Barberton greenstone belt, South Africa. Precambr. Res. 106, 93–116. Westall, F., Cavalazzi, B., Lemelle, L., Marrocchi, Y., Rouzaud, J.N., Simionovici, A., Salomé, M., Mostefaoui, S., Andreazza, C., Foucher, F., Toporski, J., Jauss, A., Thiel, V., Southam, G., MacLean, L., Wirick, S., Hofmann, A., Meibom, A., Robert, F., Défarge, C., 2011. Implications of in situ calcification for photosynthesis in a ~3.3 Ga-old microbial biofilm from the Barberton Greenstone Belt, South Africa. Earth Planet. Sci. Lett. 310, 468–479.
Westall, F., Campbell, K.A., Bréhéret, J.G., Foucher, F., Gautret, P., Hubert, A., Sorieul, S., Grassineau, N., Guido, D.M., 2015. Archean (3.33 Ga) microbe-sediment systems were diverse and flourished in a hydrothermal context. Geology 43, 615–618. Wheat, C.G., Mottl, M.J., Rudnicki, M., 2002. Trace element and REE composition of a low-temperature ridge-flank hydrothermal spring. Geochim. Cosmochim. Acta 66, 3683–3705.
Xie, X., Byerly, G.R., Ferrell Jr., R.E., 1997. IIb trioctahedral chlorite from the Barberton greenstone belt: Crystal structure and rock composition constraints with implications to geothermometry. Contrib. Miner. Petrol. 126, 275–291.